2-13-2016

# Shape Representation Using the Helmholtz Equation

Laura A. Rolston

# Shape Representation Using the Helmholtz Equation

by

Laura A. Rolston

A Thesis Submitted in Partial Fulfillment of the Requirements
for the Degree of Master of Science in Applied Mathematics
School of Mathematical Sciences, College of Science

Rochester Institute of Technology
Rochester, NY

February 13, 2016

# Committee Approval:

R·I·T
College of
Science

---

Nathan Cahill, PhD. Date
School of Mathematical Sciences
Thesis Advisor

---

Kara Maki, PhD. Date
School of Mathematical Sciences
Committee Member

---

James Marengo, PhD. Date
School of Mathematical Sciences
Committee Member

---

David Ross, PhD. Date
School of Mathematical Sciences
Committee Member

---

Elizabeth Cherry, PhD. Date
School of Mathematical Sciences
Director, MS Program in Applied and
Computational Mathematics

**Abstract**

Image classification uses a learning procedure to predict class labels based on quantitative characteristics of an image. Typical approaches involve first extracting features from a set of labeled images and using a subset of those images and their features as a "training set" to train a classifier. The classifier is then applied to the test images to predict their labels. In this thesis, we focus on *shape* classification and propose new features to be used for classifying binary images. Specifically, we propose new features based on the hitting time distribution of a Brownian motion process defined on the shape.

It has been shown that the expected time for a particle undergoing Brownian motion to hit the boundary of the shape given that the particle originated at a point $x$ inside the shape can be determined from the solution to a Poisson equation with homogeneous Dirichlet boundary conditions on the shape boundary. We now consider Brownian motion that originates *outside* the shape. To prevent this Brownian motion from continuing infinitely, we introduce an exponential dying time for the particle, and we derive the distribution of the random variable representing the minimum of the dying time and the boundary hitting time, given that the Brownian motion originates at $\mathbf{x}$. We show that the expected value, expressed as a function of $\mathbf{x}$, satisfies the Helmholtz equation.

Finally, we show how moments of this new random variable can be used as quantitative features in two classification experiments, using natural silhouettes and handwritten numerals. We show that improved results are possible when the features computed based on Brownian motion originating outside a shape are appended to those inside the shape.

# Contents

# I. Introduction

The core problem at the heart of the entire computer vision field is *image understanding*; namely, creating algorithms by which a computer can determine, at a high level, the content represented in the image. While humans are naturally able to understand images with ease, mathematical models of how this understanding occurs are still in their infancy. The field of machine learning offers possibilities for image understanding: by using exemplar images having known properties to train a classifier, new images can be classified.

In this thesis, we focus on one subset of computer vision: the classification of "shape" in images. Humans can easily look at binary silhouettes of different animals and discern differences between horses, dogs, cats and elephants, and they can instantaneously classify handwritten digits. However, human vision is time consuming and therefore costly, so we aim to accomplish the task with computer vision.

Typical computer vision image classification approaches involve (i) constructing a set of images having known labels describing the content of the image (e.g. horse, dog, cat), (ii) extracting descriptive features from each image in the set, (iii) partitioning the set into two subsets: a "training set" and a "testing set", (iv) using the features extracted from the training set to train a classifier, and (v) applying the classifier to the images in the testing set to predict their label. Our focus here is on (ii), as we propose a new set of descriptive features of a shape to be used in classification. There is a need to develop methods of shape representation to better capture shape properties for later use in classification. With improved shape representations, we can improve the accuracy of shape classification algorithms that group images based on those representations. We aim to develop a useful shape representation and show the effectiveness of those features when used in a classification experiment.

Many methods of shape representation have been previously explored. A desirable shape representation scheme is able to be used for accurate shape classification, and is invariant to scale and rotation. Previous work includes methods such as the symmetric axis transform and recognition by components, which are discussed in further detail in Chapter II.

In Chapter III, the analysis is restricted to points inside a shape. We discuss an established shape representation approach based on Brownian motion. Consider a particle originating at a point $\mathbf{x}$ inside a shape silhouette. It has been previously shown that the expected time for this particle undergoing Brownian motion to hit the boundary of the shape can be determined from

the solution to a partial differential equation called the Poisson equation. We define the survival function initial value problem and then compute moments of the survival function as descriptive quantitative features of shape silhouettes. We then use these features in classification experiments and demonstrate their efficacy.

In Chapter IV, we extend it to consider Brownian motion that originates *outside* the shape. To prevent this Brownian motion from continuing infinitely, we introduce an exponential dying time for the particle. This dying time can be considered a natural lifetime, such that the particle's motion will cease when it either hits the shape boundary or when it reaches its dying time. We then derive the distribution of the random variable representing the minimum of the dying time and the boundary hitting time, given that the Brownian motion originates at $\mathbf{x}$. We show that the expected value of this random variable, expressed as a function of $\mathbf{x}$, satisfies the Helmholtz equation. Then, we compute the moments of the random variable, discretize the initial boundary value problem as well as the moments, and provide both analytical and computational examples of these moments for various shapes.

Finally, Chapter V demonstrates the utility of the new shape representation in a classification experiment. We show how moments of this random variable can be used as quantitative features for shape classification.

## II. Related Work

Properties of a shape can be extracted from its silhouette and used in shape classification. Blum's early work [5] develops the medial axis function for extracting the skeleton of a shape. The skeleton, or medial axis, is the locus of points equidistant from the shape boundary. The medial axis function is a symmetrical central description of a shape whose boundary is a closed contour. The medial axis function is further explored in [6] with the symmetric axis transform, which describes the shape of an object using the intersection of a collection of discs, comprising the skeleton, shown in Figure 1. The medial axis shape representation is also adapted in [27] to better represent shapes with boundary noise, and in [17] is extended to extracting skeletons of arbitrary 3D objects, as shown in Figure 2. Skeleton-based representations followed [5], including thinning algorithms such as [22] and Voronoi diagrams.

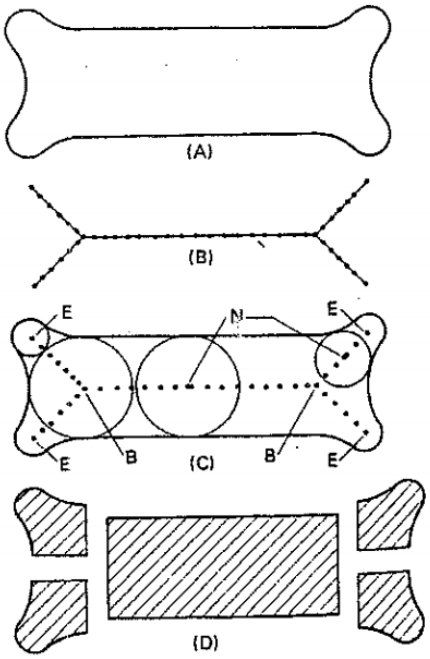


**Figure 1:** A bone shape (A) and its medial axis (B). (C) shows the medial axis function derived as the locus of centers of discs inscribed in the image. In (D), the shape is partitioned into segments. Image taken from [5].

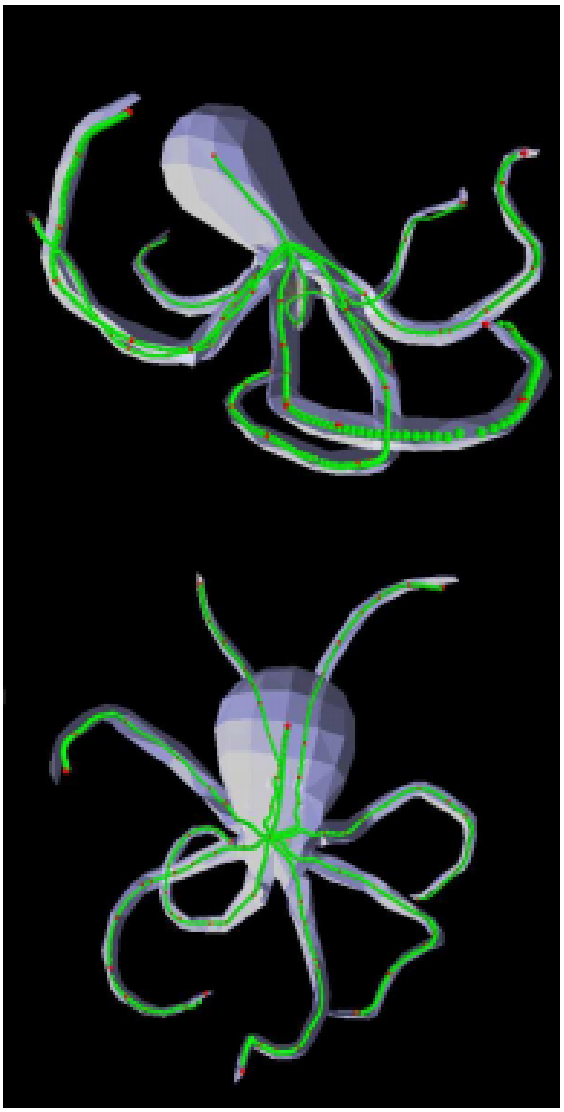

**Figure 2:** Skeleton extracted from 3D model. Image taken from [17].

Another explicit approach for shape representation is the part-based representation, where an object is described by a collection of primitive shapes. Marr and Nishikara [19] explore a part-based representation of three dimensional shapes. Biederman [3] focuses on human shape recognition based on the simple geometric components of a shape. This Recognition-By-Components approach is further explored in Pentland [23] where it is optimized for computer vision, and Siddiqi and Kimia [28] expand it's ability to remain invariant to local deformations and global changes such as translations, rotations and scalings.

In contrast to explicit methods for shape representation, implicit methods have also been explored. The Euclidean distance transform computes the minimum distance from each point inside a shape to the boundary of the shape. Algorithms for the Euclidean distance transform are presented in Fabbri *et al* in [10], and an example is shown in Figure 3. More distance based transforms are explored in [33], as shown in Figure 4. This concept is applied in the development of Voronoi diagrams in [11], [21] and [20], shown in Figure 5.

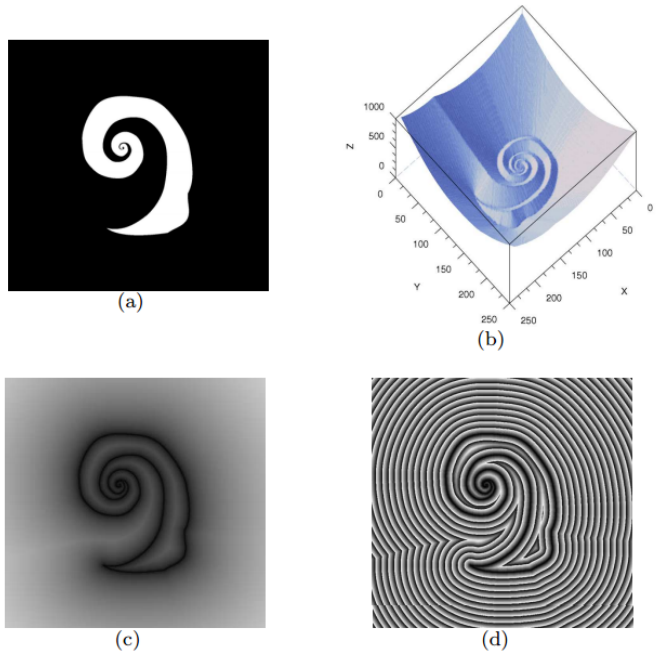


**Figure 3:** A spiraled shape (a), its distance transform, where the smallest distance from each point to the border is represented by the height of a surface (b) and alternately with brightness (c) and corresponding iso-distance curves (d). Image taken from [10].

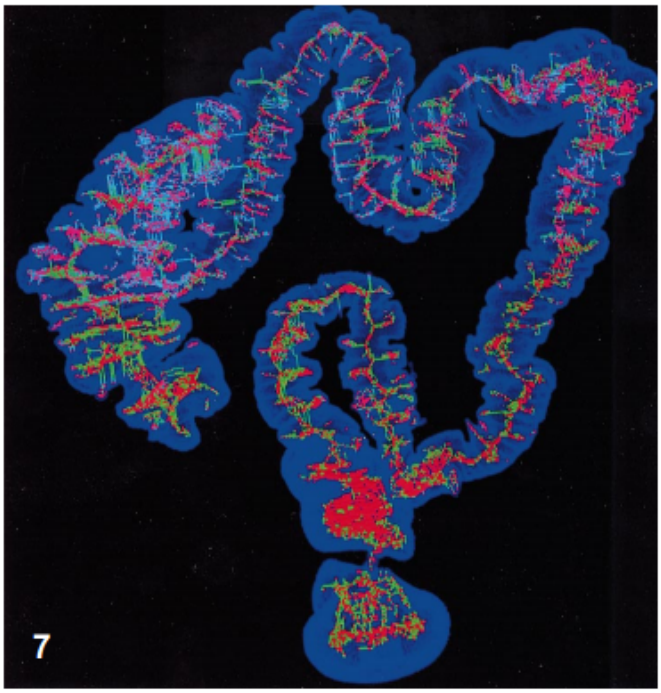


**Figure 4:** Skeleton extraction used for centerline generation in colon image. Image taken from [33].

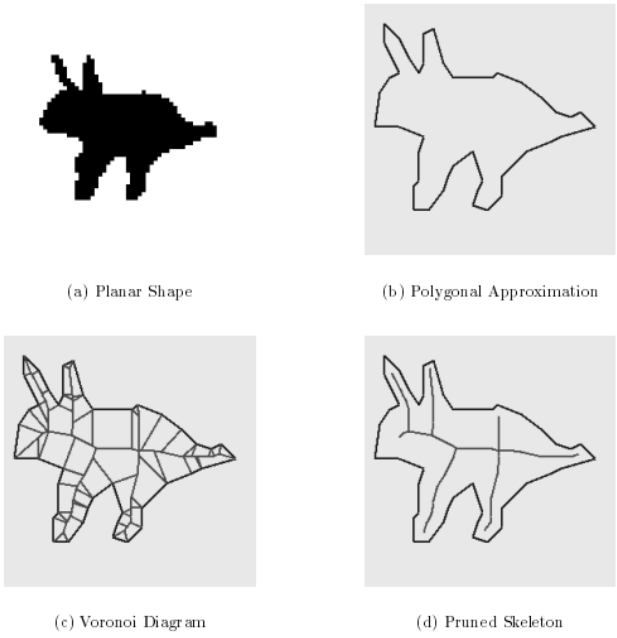


**Figure 5:** Voronoi diagram and pruned skeleton representation of image. The pruned skeleton is determined by removing relatively unimportant sections from the full Voronoi diagram to obtain a more basic shape representation. Image taken from [20].

Also citing [5], [25] presents Deformable Shape Loci (DSL) as a representation and segmentation method for 2D and 3D medical images. This is extended in [24], where M-reps are presented as a means for modeling 3D solids based on the medial axis transform, shown in Figure 6. M-reps are applied to medical images of kidneys, hippocampi and corpus collosa in [26], [12] and [29], respectively. Figure 7 shows an example of M-reps applied to an image of a kidney.

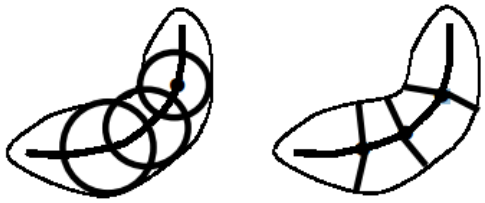

**Figure 6:** 2D illustration of (left) the traditional view of the medial locus, bitangent to the object boundary. The equivalent as an M-rep (right): a curve of hubs at the sphere center and equal length spokes normal to object boundary. Image taken from [24].

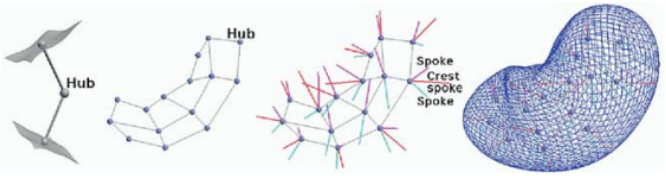


**Figure 7:** Surface rendering using M-reps. Image taken from [26].

In [14], a new implicit method for extracting properties from a shape is presented. A function is defined on the shape; the value of the function at a particular point is the expected time that a symmetric random walk takes to hit the boundary, given it started at that point. The authors of [14] show that the function is actually the solution to a nonhomogeneous Poisson equation on the shape, with homogeneous Dirichlet boundary conditions. Examples of the solution to the Poisson equation on shapes are shown in Figures 8 and 9. Figure 8 illustrates the advantage of this representation: it is smooth and thus differentiable on the shape interior, whereas the Eucludean distance transform is not.

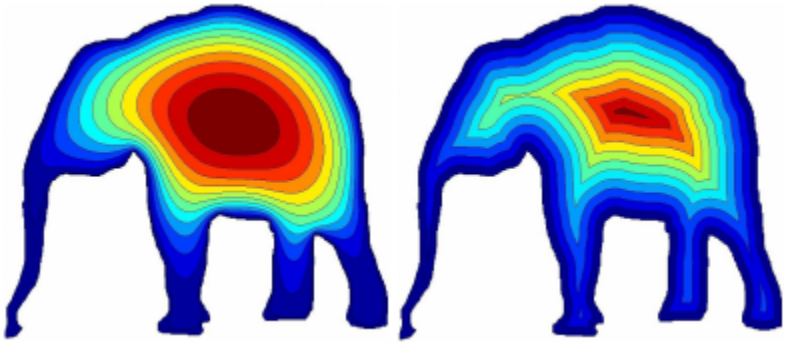

**Figure 8:** Left: level sets of the solution to the Poisson equation for the shape of an elephant. Right: the level sets of the distance transform for the same shape. Image taken from [14].

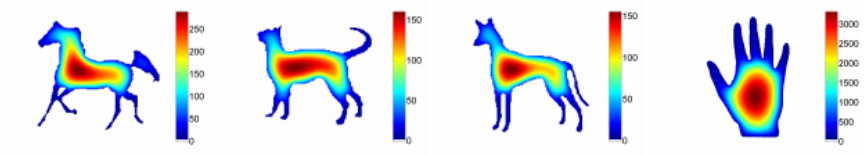

**Figure 9:** Solution to the Poisson equation for natural silhouettes. Image taken from [14].

The random walk approach of [14] is extended in [15], where a graph based image segmentation algorithm is presented. Similar to the method presented in the following chapters, it utilizes Laplace's equation. In addition, [2] uses this method to extract space-time features of human motion, and [13] extends it by implementing Robin boundary conditions. In [32], the random walk approach is applied to gait recognition. Each frame of a video of a person's walk are taken and properties of the images are extracted. Similarly, [4] applies random walks to extract properties of shapes created as a person runs, walks or does jumping jacks, shown in Figure 10. The random walk method introduced in [14] is applied to 3D face recognition in [18]. While these methods focus on functions inside shapes, functions on surfaces can be used shape recognition, specifically 3D face recognition as shown in [7] and [9].

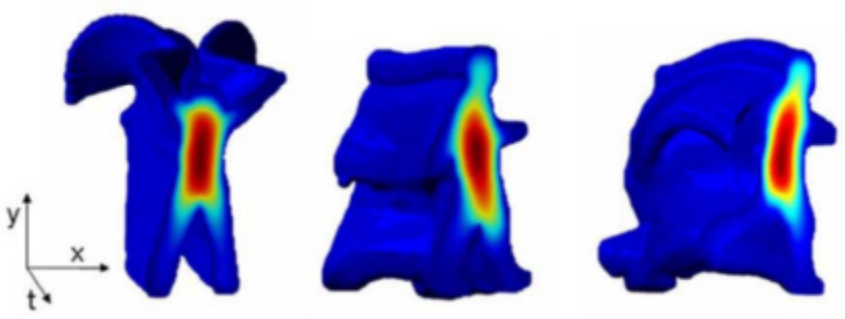


**Figure 10:** The solution to the Poisson equation on jumping jack, walking and running space time shapes. Image taken from [4].

The shape representation given in [14] utilized the Poisson equation in computing the mean hitting time for any point inside a shape. A question that follows naturally is whether or not the same computation can be done on the outside of the shape. In the following chapters, we utilize the idea of a hitting time, as introduced in [14], which was focused on deriving and analyzing the Poisson function and its properties on the inside of a shape. We extend this idea to develop a representation that can be computed on the outside as well as the inside of the shape.

# III. Brownian Motion Hitting Times

We first consider the case where a particle originates at a point in the interior of the shape and undergoes Brownian motion. The hitting time of the particle is defined as the first time the particle hits the boundary of the shape. We are interested in the distribution of hitting time given that the Brownian motion originates at a specific position $\mathbf{x}$ inside the shape.

Now, consider a shape that has been sampled on a uniformly spaced grid. The method developed by Gorelick et al [14] utilizes the notion of random walks to extract properties of a silhouette. These properties are defined by the expected duration of the random walks originating at points in the shape interior.

In this chapter, we extend the analysis of [14] to show how the survival function of the Brownian motion hitting time is the solution to a boundary value problem on the shape. In Section III.2, the moments of the hitting time are computed from the survival function. Examples are shown in Section III.3.

To formalize the concept of shape, we define a shape as a compact set $\bar{\Omega} \subset \mathbb{R}^n$, and we denote the interior and boundary of the shape by $\Omega$ and $\partial\Omega$, respectively. To formalize the concept of hitting time, let $\{X(t) \in \mathbb{R}^n, t \geq 0\}$ denote the position of a particle undergoing Brownian motion, and let $T_B$ be defined as follows:

$$T_B = \begin{cases} \inf_{t\geq 0}\{t | X(t) \in \mathbb{R}^n \backslash \bar{\Omega}\}, & X(0) \in \Omega, \\ \inf_{t\geq 0}\{t | X(t) \in \bar{\Omega}\}, & X(0) \in \mathbb{R}^n \backslash \bar{\Omega}. \end{cases}$$

Therefore, $T_B$ can be thought of as a *hitting time*; namely, $T_B$ is the first time that the particle hits the boundary of the shape. We begin by considering only the particles that start inside the shape (i.e., $X(0) \in \bar{\Omega}$), in which case $T_B$ is the first exit time of the particle from $\bar{\Omega}$.

## III.1 Survival Function Initial Boundary Value Problem

For any point $\mathbf{x} \in \mathbb{R}^n$, we define the *survival function* $S(\mathbf{x}, t)$ to be the probability that the hitting time exceeds $t$ given that the particle is initially located at $\mathbf{x}$; that is,

$$S(\mathbf{x}, t) = P(T_B > t | X(0) = \mathbf{x}). \tag{III.1}$$

As shown in Appendix A.1.1, for points $\mathbf{x} \in \bar{\Omega}$, the survival function in $n$ dimensions satisfies the initial boundary value problem (IBVP):

$$\begin{aligned} \frac{\partial}{\partial t} S(\mathbf{x}, t) - \frac{1}{2n} \Delta S(\mathbf{x}, t) = 0, \quad \forall \mathbf{x} \in \Omega, \quad t \geq 0, \\ S(\mathbf{x}, t) = 0, \quad \forall \mathbf{x} \in \partial\Omega, \quad t \geq 0, \\ S(\mathbf{x}, 0) = 1, \quad \forall \mathbf{x} \in \Omega. \end{aligned} \tag{III.2}$$

Now, we define the operator $\mathcal{L}$ by:

$$\mathcal{L}\{S(\mathbf{x}, t)\} = \frac{\partial}{\partial t} S(\mathbf{x}, t) - \frac{1}{2n} \Delta S(\mathbf{x}, t)\,. \tag{III.3}$$

(III.2) can then be rewritten as:

$$\begin{aligned} \mathcal{L}\{S(\mathbf{x}, t)\} = 0, \quad \forall \mathbf{x} \in \Omega, \quad t \geq 0, \\ S(\mathbf{x}, t) = 0, \quad \forall \mathbf{x} \in \partial\Omega, \quad t \geq 0, \\ S(\mathbf{x}, 0) = 1, \quad \forall \mathbf{x} \in \Omega. \end{aligned} \tag{III.4}$$

## III.2 Moments

The $k^{th}$ moment about zero of the hitting time $T_B$ of the Brownian motion starting at point $\mathbf{x}$ inside the shape can be computed from the survival function by:

$$U_k(\mathbf{x}) = k \int_0^\infty t^{k-1} S(\mathbf{x}, t)\, dt. \tag{III.5}$$

We show in Appendix A.1.2 that multiplying each side of (III.2) by $kt^{k-1}$, integrating, and employing (III.5) yields the recursive set of boundary value problems:

$$\begin{aligned} -\frac{1}{2n} \Delta U_k(\mathbf{x}) = k U_{k-1}(\mathbf{x})\,, \quad \forall \mathbf{x} \in \Omega, \\ U_0(\mathbf{x}) = 1, \quad \forall \mathbf{x} \in \Omega, \\ U_k(\mathbf{x}) = 0, \quad \forall \mathbf{x} \in \partial\Omega, \end{aligned} \tag{III.6}$$

for k= 1,2,....

Note that when $k = 0$ , the zeroth moment of $U_0(\mathbf{x}) = 1$, as $E[T_B^0] = 1$.

Central moments, denoted $V_k(\mathbf{x})$ can then be computed as:

$$V_k(\mathbf{x}) = \sum_{m=0}^{k} \binom{k}{m} (-1)^{k-m}\, U_m(\mathbf{x})\, U_1(\mathbf{x})^{k-m}\,. \tag{III.7}$$

Standardized moments $W_k(\mathbf{x})$ can then be computed from the central moments as follows:

$$W_k(\mathbf{x}) = \frac{V_k(\mathbf{x})}{{V_2}^{k/2}}. \tag{III.8}$$

For example, the standard deviation, skewness, and kurtosis are given by:

$$W_2(\mathbf{x}) = \sqrt{V_2(\mathbf{x})}, \tag{III.9}$$

$$W_3(\mathbf{x}) = \frac{V_3(\mathbf{x})}{V_2(\mathbf{x})^{3/2}}, \tag{III.10}$$

$$W_4(\mathbf{x}) = \frac{V_4(\mathbf{x})}{V_2(\mathbf{x})^2}, \tag{III.11}$$

respectively.

## III.3 Computational Examples of Moments

In this section, we illustrate the hitting time and higher moments defined in Section III.2 for a shape that represents a silhouette of a horse.

The mean hitting time $U_1(\mathbf{x})$, is shown in Figure 11. The standardized moments of the hitting time, computed from the central moments as in (III.9) through (III.11) and denoted $W_k(\mathbf{x})$ are shown (along with variance) in Figure 12. The moments about zero $U_k(\mathbf{x})$, and central moments $V_k(\mathbf{x})$ are shown in Figures 13 and 14, respectively.

The level sets of $U_k(\mathbf{x})$, $V_k(\mathbf{x})$ and $W_k(\mathbf{x})$ are smoothed versions of the bounding contour. The head, legs and tail exhibit much smaller values than those inside the torso for the moments about zero, $U_k(\mathbf{x})$, the central moments, $V_k(\mathbf{x})$, and the standard deviation $W_2(\mathbf{x})$. The skewness, $W_3(\mathbf{x})$ and kurtosis, $W_4(\mathbf{x})$ achieve maximum values on the ears, tail and legs while the values in the torso are relatively small. Notice that the skewness and kurtosis values are noisy on the boundaries of the shape and there are points with values much larger than the surrounding values, so it is difficult to visualize the results. We found that using the reciprocals of the skewness and kurtosis provides a better visualization. The reciprocal of the skewness and kurtosis, $\frac{1}{W_3(\mathbf{x})}$ and $\frac{1}{W_4(\mathbf{x})}$, respectively, achieve maximum values both near the centroid, similar to $U_k(\mathbf{x})$ and $V_k(\mathbf{x})$, but also on the feet and tail.

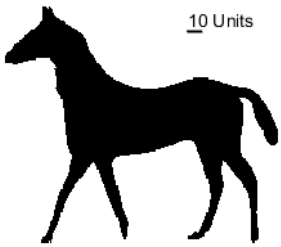


Silhouette

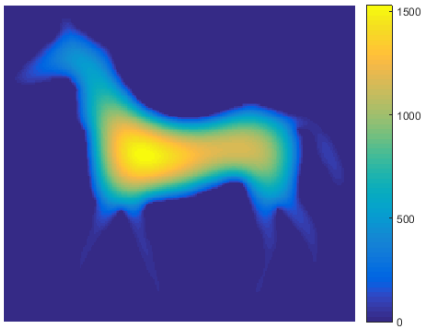


Mean

$U_1(\mathbf{x})$

**Figure 11:** Mean Hitting Time of $T_B$ where $X(0) \in \bar{\Omega}$.

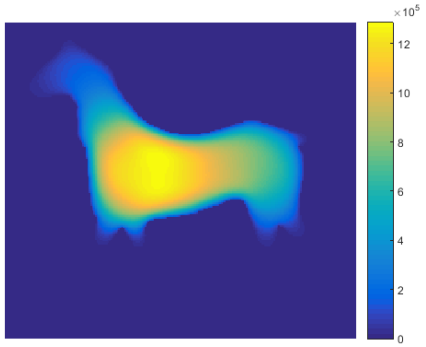


Variance

$V_2(\mathbf{x})$

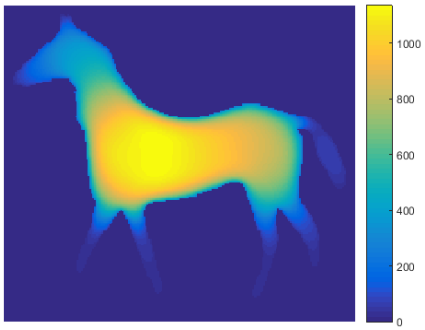


Standard Deviation

$W_2(\mathbf{x})$


Skewness

$W_3(\mathbf{x})$

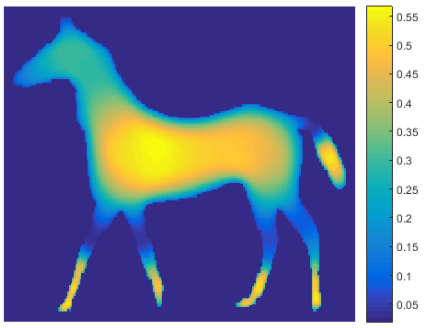


Reciprocal of Skewness

$\frac{1}{W_3(\mathbf{x})}$

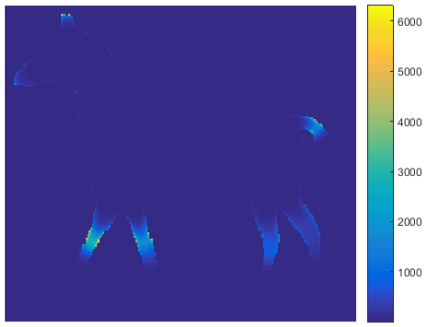


Kurtosis

$W_4(\mathbf{x})$

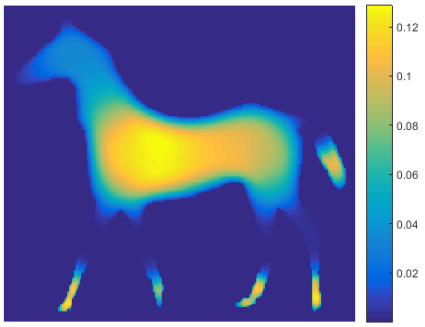


Reciprocal of Kurtosis

$\frac{1}{W_4(\mathbf{x})}$

**Figure 12:** Moments of $T_B$ where $X(0) \in \bar{\Omega}$.

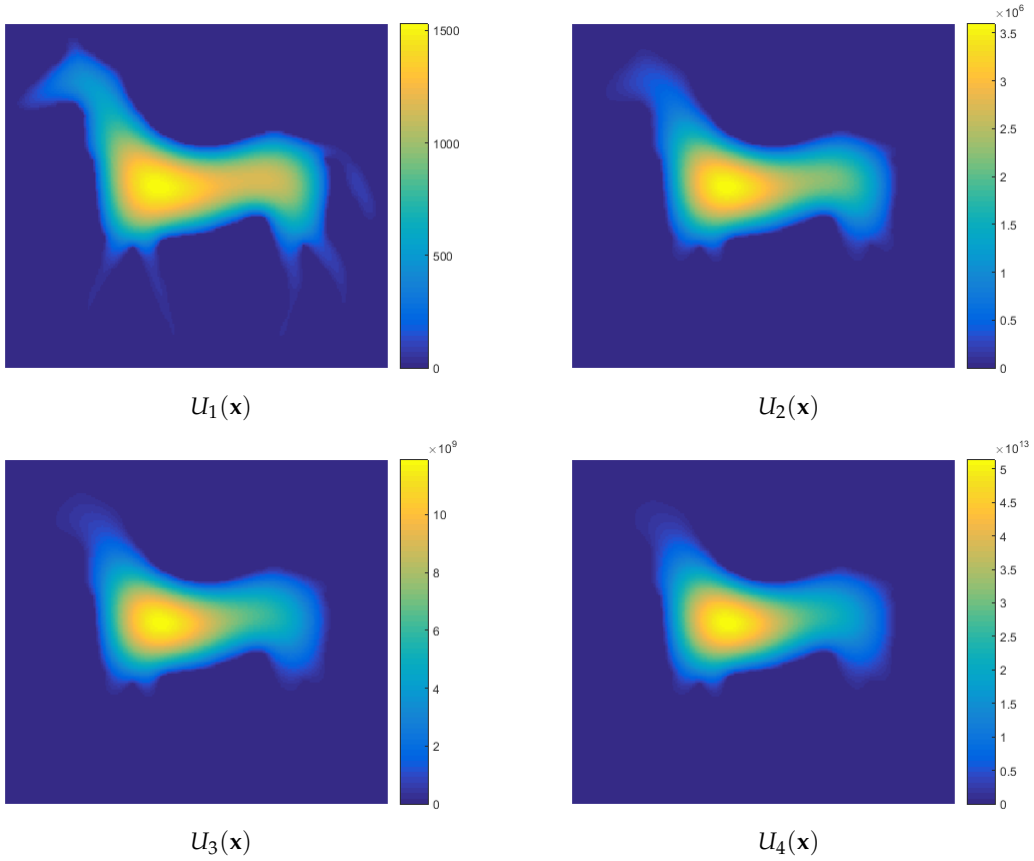


**Figure 13:** $k^{th}$ Moments About Zero of $T_B$ where $X(0) \in \bar{\Omega}$.

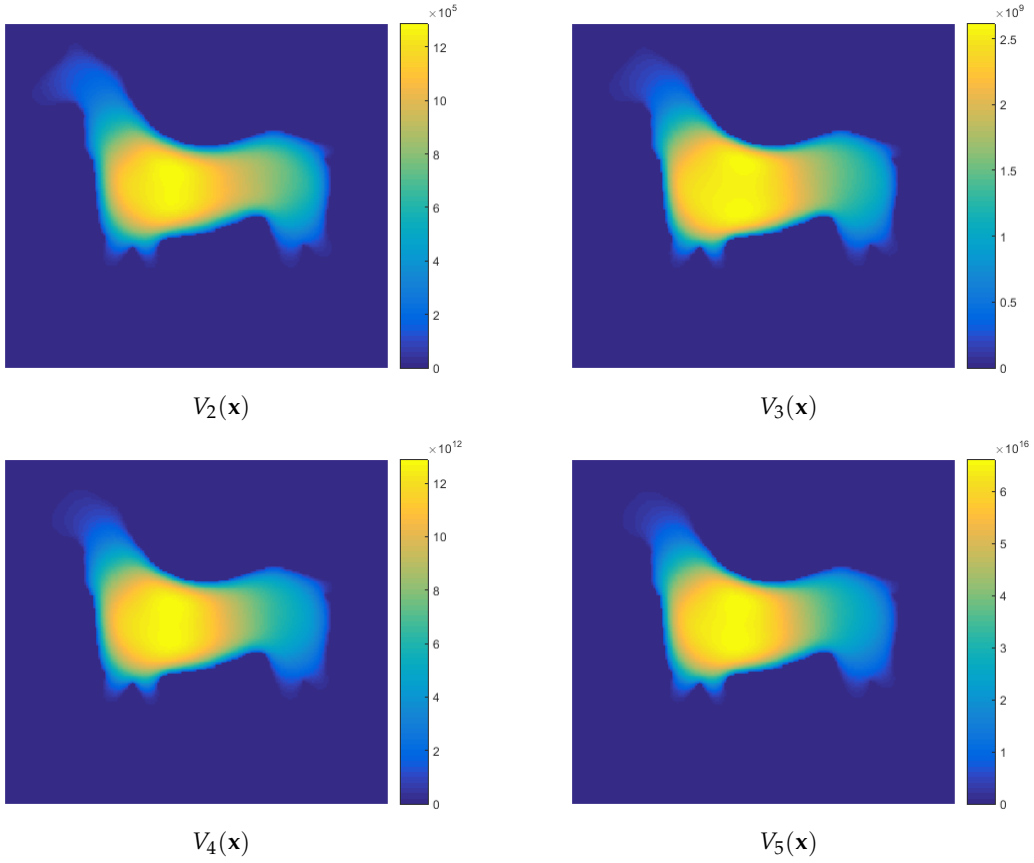


$V_2(\mathbf{x})$ $V_3(\mathbf{x})$

$V_4(\mathbf{x})$ $V_5(\mathbf{x})$

**Figure 14:** $k^{th}$ Central Moments of $T_B$ where $X(0) \in \bar{\Omega}$.

In Figures 15 and 16, the probability density function and cumulative distribution function of $T_B$ are computed for various points on the head, neck, leg and centroid of a horse silhouette.

Notice that $T_B$ takes on smaller values when the random walk begins at a point in an extremity of the horse such as at point C or D, shown in Figures 16, compared to those that begin at points in the torso or neck like points A and B, as in Figure 15.

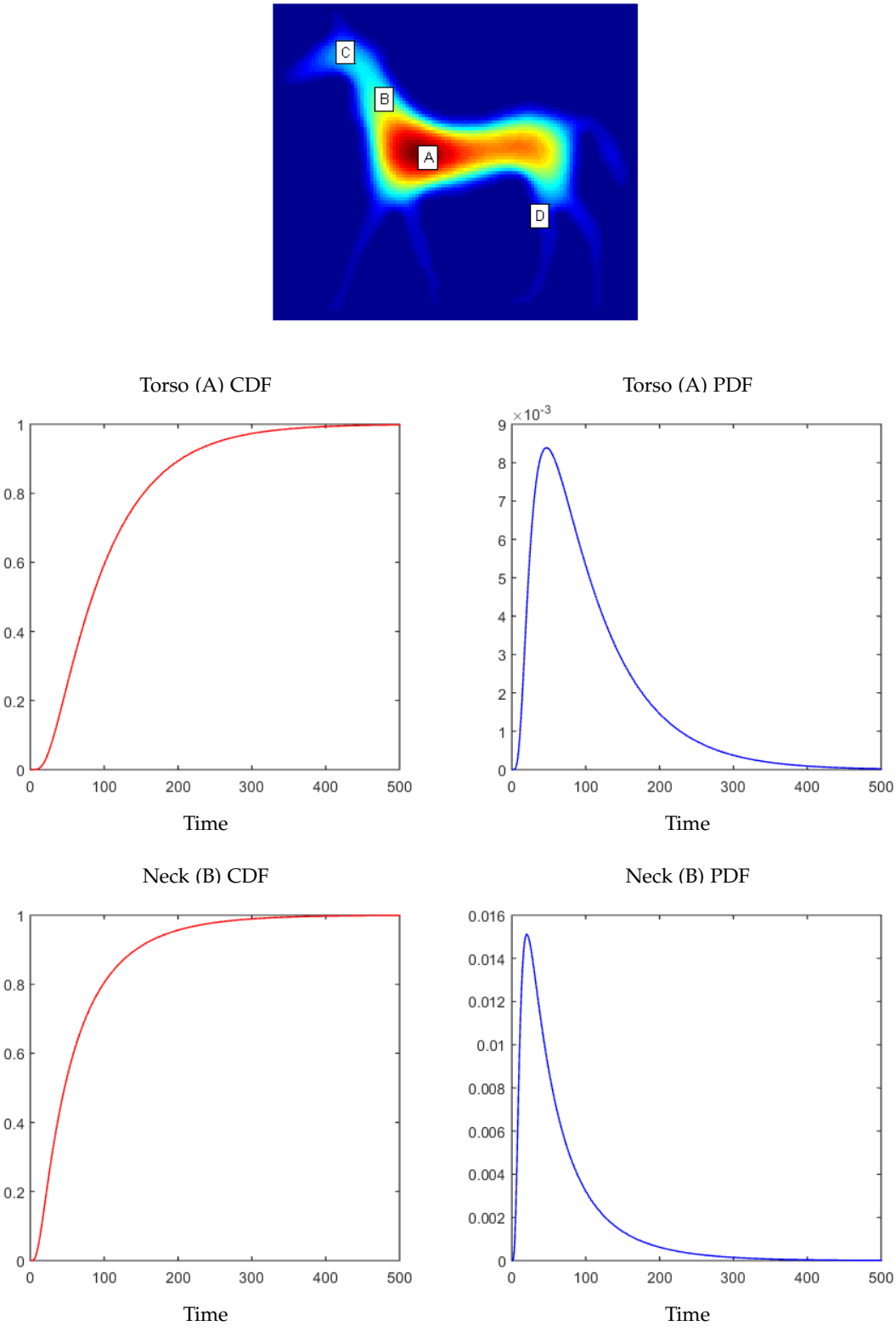


**Figure 15:** CDF and PDF of random walk hitting times given initial positions at points A and B.

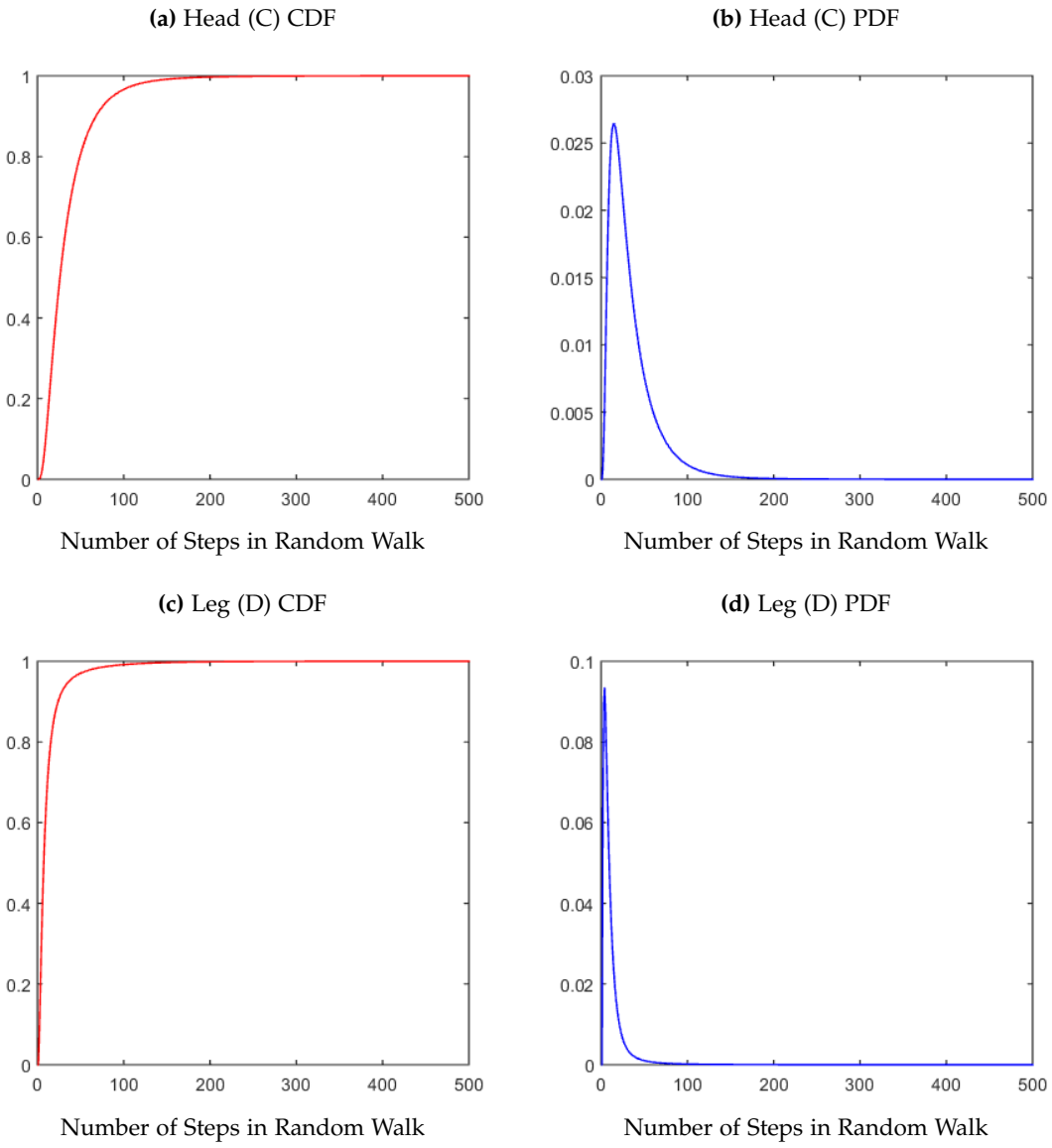


**Figure 16:** CDF and PDF of random walk hitting times given initial positions at points C and D.

# IV. Brownian Motion Augmented with Natural Lifetime

In Chapter III, we considered representations that are defined only on a closed shape. In this chapter, we expand these representations to be defined everywhere in $\mathbb{R}^n$, including the shape exterior.

Random walks in two dimensions are null recurrent, meaning the probability that the random walk will return to its starting position is equal to one, however, the expected value of the number of steps it takes to return to that position is infinite. This implies that the mean hitting time is infinite, and is not useful in providing a representation whose values outside the shape can be used to discriminate between different shapes. (Note that random walks in three dimensions or higher are transient).

As an alternative to using the mean hitting time alone, we assign to the particle an exponentially distributed lifetime $T_L$, that is independent of $X(t)$, guaranteeing that the Brownian motion will eventually terminate. Incorporating this dying time, or natural lifetime, allows us to measure the minimum of the times required to $(1)$ hit the boundary of the shape, as in the previous section, or $(2)$ reach the end of its natural lifetime, and this new quantity will have a finite expected value.

In this section, we derive an initial boundary value problem describing the survival function for the minimum of $T_B$ and $T_L$. We then illustrate some properties.

## IV.1 Survival Function Initial Boundary Value Problem

As in Section III.1, we define a shape as a compact set $\bar{\Omega} \subset \mathbb{R}^n$, and denote the interior by $\Omega$ and boundary by $\partial\Omega$. Again we consider a particle undergoing Brownian motion, and denote the position of the particle $\{X(t), t \geq 0\}$. Recall the hitting time of the particle, $T_B$, defined as the first time at which the particle crosses the boundary of the shape, i.e.

$$T_B = \begin{cases} \inf_{t\geq 0}\{t | X(t) \in \mathbb{R}^n \backslash \bar{\Omega}\}, & X(0) \in \Omega, \\ \inf_{t\geq 0}\{t | X(t) \in \bar{\Omega}\}, & X(0) \in \mathbb{R}^n \backslash \bar{\Omega}. \end{cases}$$

In the previous case described in Section III.1, the hitting time function $S(\mathbf{x}, t)$ is defined as the probability that the hitting time exceeds $t$ given that the particle is initially located at $\mathbf{x}$. Now,

define $T_L$ to be the natural lifetime of the particle. We will assume that $T_L$ is independent of $X(t)$ and $T_B$ and that $T_L$ has an exponential distribution with parameter $\lambda$, so that $P(T > t) = e^{-\lambda t}$ for $t \geq 0$ and 1 otherwise.

Now, we define $T = \min(T_B, T_L)$, and we define $S_\beta(\mathbf{x}, t)$ to be the probability that the minimum of the hitting time and the lifetime exceeds $t$, given that the particle is initially located at $\mathbf{x}$, and $\beta = \frac{1}{\lambda} = E[T_L]$. That is:

$$S_\beta(\mathbf{x}, t) = P\Big(T > t | X(0) = \mathbf{x}, T_L \sim \exp\Big(\tfrac{1}{\beta}\Big)\Big). \tag{IV.1}$$

As shown in Appendix A.2.1, for points $\mathbf{x} \in \mathbb{R}^n \backslash \bar{\Omega}$, the survival function $S_\beta(\mathbf{x}, t)$ can be written as the following initial boundary value problem:

$$\begin{aligned} \frac{\partial}{\partial t} S_\beta(\mathbf{x}, t) - \frac{1}{2n} \Delta S_\beta(\mathbf{x}, t) + \frac{1}{\beta} S_\beta(\mathbf{x}, t) = 0, \quad \forall \mathbf{x} \in \mathbb{R}^n \backslash \partial\Omega, \quad t \geq 0, \\ S_\beta(\mathbf{x}, t) = 0, \quad \forall \mathbf{x} \in \partial\Omega, \quad t \geq 0, \\ S_\beta(\mathbf{x}, 0) = 1, \quad \forall \mathbf{x} \in \Omega. \end{aligned} \tag{IV.2}$$

Applying the definition of $\mathcal{L}$ from (III.3) allows us to write (IV.2) as:

$$\begin{aligned} \left(\mathcal{L} + \frac{1}{\beta} I\right) \{S_\beta(\mathbf{x}, t)\} = 0, \quad \forall \mathbf{x} \in \mathbb{R}^n \backslash \partial\bar{\Omega}, \quad t \geq 0, \\ S_\beta(\mathbf{x}, t) = 0, \quad \forall \mathbf{x} \in \partial\Omega, \quad t \geq 0, \\ S_\beta(\mathbf{x}, 0) = 1, \quad \forall \mathbf{x} \in \Omega. \end{aligned} \tag{IV.3}$$

In the following sections, we examine various properties of $T$ given $X(0)$.

## IV.2 Moments

The $k^{\text{th}}$ moment of $T$ given $X(0) = \mathbf{x}$ is denoted by $U_k(\mathbf{x})$, and can be computed from the survival function by:

$$U_{k,\beta}(\mathbf{x}) = k \int_0^\infty t^{k-1} S_\beta(\mathbf{x}, t)\, dt. \tag{IV.4}$$

As shown in Appendix A.2.2, by multiplying both sides of the inital boundary value problem (IV.2) by $kt^{k-1}$ and then integrating, we can employ (IV.4) and obtain the following boundary

value problem:

$$-kU_{k-1,\beta}(\mathbf{x}) - \frac{1}{2n}\Delta U_{k,\beta}(\mathbf{x}) + \frac{1}{\beta}U_{k,\beta}(\mathbf{x}) = 0, \quad \forall \mathbf{x} \in \mathbb{R}^n \backslash \partial\Omega,$$
$$U_{k,\beta}(\mathbf{x}) = 0, \quad \forall \mathbf{x} \in \partial\Omega,$$
$$U_{0,\beta}(\mathbf{x}) = 1, \quad \forall \mathbf{x} \in \mathbb{R}^n. \tag{IV.5}$$

or:

$$-kU_{k-1,\beta}(\mathbf{x}) + \left(\frac{1}{\beta}I - \frac{1}{2n}\Delta\right) U_{k,\beta}(\mathbf{x}) = 0, \quad \forall \mathbf{x} \in \mathbb{R}^n \backslash \partial\Omega,$$
$$U_{1,\beta}(\mathbf{x}) = \beta, \quad \forall \mathbf{x} \in \partial\Omega, \tag{IV.6}$$

where $\beta$ is the expected value of exponentially distributed random variable $T_L$ the natural lifetime of the particle.

Notice that when $k = 1$, (IV.5) can be rewritten as the following Helmholtz equation:

$$\Delta U_{1,\beta}(\mathbf{x}) - \frac{2n}{\beta}U_{1,\beta}(\mathbf{x}) = -2n, \quad \forall \mathbf{x} \in \mathbb{R}^n \backslash \partial\Omega,$$
$$U_{1,\beta}(\mathbf{x}) = \beta, \quad \forall \mathbf{x} \in \partial\Omega. \tag{IV.7}$$

Central moments, denoted $V_k(\mathbf{x})$, can then be computed as:

$$V_{k,\beta}(\mathbf{x}) = \sum_{m=0}^{k} \binom{k}{m} (-1)^{k-m} U_{m,\beta}(\mathbf{x}) \, U_{1,\beta}(\mathbf{x})^{k-m}, \quad k = 1, 2, ... \tag{IV.8}$$

Standardized moments $W_{k,\beta}(\mathbf{x})$ can then be computed from the central moments as follows:

$$W_{k,\beta}(\mathbf{x}) = \frac{V_{k,\beta}(\mathbf{x})}{V_{2,\beta}(\mathbf{x})^{\frac{k}{2}}}, \quad k = 1, 2, ... \tag{IV.9}$$

## IV.3 Discretization of IBVP

Recall (IV.2), the initial boundary value problem:

$$\frac{\partial}{\partial t}S_\beta(\mathbf{x}, t) - \frac{1}{2n}\Delta S_\beta(\mathbf{x}, t) + \frac{1}{\beta}S_\beta(\mathbf{x}, t) = 0, \quad \forall \mathbf{x} \in \mathbb{R}^n \backslash \partial\Omega, \quad t \geq 0,$$
$$S_\beta(\mathbf{x}, t) = 0, \quad \forall \mathbf{x} \in \partial\Omega, \quad t \geq 0,$$
$$S_\beta(\mathbf{x}, 0) = 1, \quad \forall \mathbf{x} \in \bar{\Omega}.$$

In this section we discretize this IBVP both in space and in time.

### IV.3.1 Spatial Discretization

Suppose $\bar{\Gamma} \subset \bar{\Omega}$ is a $n$-dimensional uniform grid of points. Each grid point $\mathbf{x}$ has neighborhood $\mathcal{N}(\mathbf{x}) = \bar{\Gamma} \cap \{\mathbf{x} \pm h\mathbf{e}_j | j = 1, \ldots, n\}$, where $\mathbf{e}_j$ is the $j^{\text{th}}$ column of the $n$-dimensional identity matrix, and $h$ is the grid spacing. The interior $\Gamma$ contains all points in $\bar{\Gamma}$ that have $2n$ neighbors (i.e., points for which $|\mathcal{N}(\mathbf{x})| = 2n$), and the discrete boundary $\partial\Gamma = \bar{\Gamma} \backslash \Gamma$.

We can rewrite the spatial Laplacian of the survival function as the sum of its second partial derivatives in space. For points in $\mathbb{R}^n \backslash \partial\bar{\Gamma}$ we have:

$$\Delta S_\beta(\mathbf{x}, t) = \sum_{i=1}^{n} \frac{\partial^2}{\partial x_i^2} S_\beta(\mathbf{x}, t)\,. \tag{IV.10}$$

Implementing the centered difference approximation for the second derivative gives:

$$\Delta S_\beta(\mathbf{x}, t) \approx \sum_{i=1}^{n} \frac{S_\beta(\mathbf{x} - h\mathbf{e}_i, t) - 2S_\beta(\mathbf{x}, t) + S_\beta(\mathbf{x} + h\mathbf{e}_i, t)}{h^2},$$

where $\mathbf{e}_i$ is the $i$th unit vector. That is,

$$\mathbf{e}_i = \begin{bmatrix} 0 \\ \vdots \\ 1 \\ \vdots \\ 0 \end{bmatrix},$$

where 1 is in the $i$th position of the $1 \times n$ vector $\mathbf{e}_i$.

Bringing the term $-2S_\beta(\mathbf{x}, t)$ outside the summation yields:

$$\Delta S_\beta(\mathbf{x}, t) \approx -\frac{2n}{h^2} S_\beta(\mathbf{x}, t) + \sum_{i=1}^{n} \frac{S_\beta(\mathbf{x} - h\mathbf{e}_i, t) + S_\beta(\mathbf{x} + h\mathbf{e}_i, t)}{h^2}. \tag{IV.11}$$

Substituting (IV.11) into (IV.2) gives the discrete spatial approximation:

$$\frac{\partial}{\partial t} S_\beta(\mathbf{x}, t) - \frac{1}{2n} \left[ -\frac{2n}{h^2} S_\beta(\mathbf{x}, t) + \sum_{i=1}^{n} \frac{S_\beta(\mathbf{x} - h\mathbf{e}_i, t) + S_\beta(\mathbf{x} + h\mathbf{e}_i, t)}{h^2} \right] + \frac{1}{\beta} S_\beta\left(\mathbf{x}, t\right) = 0. \tag{IV.12}$$

Simplifying gives the following:

$$\frac{\partial}{\partial t} S_\beta(\mathbf{x}, t) + \left( \frac{1}{h^2} + \frac{1}{\beta} \right) S_\beta(\mathbf{x}, t) - \frac{1}{2n} \sum_{i=1}^{n} \frac{S_\beta(\mathbf{x} - h\mathbf{e}_i, t) + S_\beta(\mathbf{x} + h\mathbf{e}_i, t)}{h^2} = 0. \tag{IV.13}$$

### IV.3.2 Time Discretization

Discretizing (IV.13) forward in time with time step $\Delta\tau$ yields:

$$\frac{S_\beta\left(\mathbf{x}, t^{k+1}\right) - S_\beta\left(\mathbf{x}, t^k\right)}{\tau} = -\left(\frac{1}{h^2} + \frac{1}{\beta}\right) S_\beta\left(\mathbf{x}, t^k\right) + \frac{1}{2nh^2}\sum_{i=1}^{n}\left[S_\beta\left(\mathbf{x} - h\mathbf{e}_i, t^k\right) + S_\beta\left(\mathbf{x} + h\mathbf{e}_i, t^k\right)\right]. \tag{IV.14}$$

Multiplying both sides of (IV.14) by $\tau$ and adding $S_\beta\left(\mathbf{x}, t^k\right)$ to both sides gives:

$$S_\beta\left(\mathbf{x}, t^{k+1}\right) = S_\beta\left(\mathbf{x}, t^k\right) - \tau\left(\frac{1}{h^2} + \frac{1}{\beta}\right) S_\beta\left(\mathbf{x}, t^k\right) + \frac{\tau}{2nh^2}\sum_{i=1}^{n}\left[S_\beta\left(\mathbf{x} - h\mathbf{e}_i, t^k\right) + S_\beta\left(\mathbf{x} + h\mathbf{e}_i, t^k\right)\right]. \tag{IV.15}$$

Combining like terms yields the explicit iteration:

$$S_\beta\left(\mathbf{x}, t^{k+1}\right) = \left(1 - \frac{\tau}{\beta} - \frac{\tau}{h^2}\right) S_\beta\left(\mathbf{x}, t^k\right) + \frac{\tau}{2nh^2}\sum_{i=1}^{n}\left[S_\beta\left(\mathbf{x} - h\mathbf{e}_i, t^k\right) + S_\beta\left(\mathbf{x} + h\mathbf{e}_i, t^k\right)\right]. \tag{IV.16}$$

Alternatively, discretizing backward in time with step size $\tau$ yields:

$$\begin{aligned}\frac{S_\beta\left(\mathbf{x}, t^{k+1}\right) - S_\beta\left(\mathbf{x}, t^k\right)}{\tau} = &-\left(\frac{1}{h^2} + \frac{1}{\beta}\right) S_\beta\left(\mathbf{x}, t^{k+1}\right) \\ &+ \frac{1}{2nh^2}\sum_{i=1}^{n}\left[S_\beta\left(\mathbf{x} - h\mathbf{e}_i, t^{k+1}\right) + S_\beta\left(\mathbf{x} + h\mathbf{e}_i, t^{k+1}\right)\right].\end{aligned} \tag{IV.17}$$

Multiplying by $-\tau$ and adding $S_\beta\left(\mathbf{x}, t^{k+1}\right)$ to both sides yields:

$$\begin{aligned}S_\beta\left(\mathbf{x}, t^k\right) = &\, S_\beta\left(\mathbf{x}, t^{k+1}\right) + \frac{\tau}{h^2} S_\beta\left(\mathbf{x}, t^{k+1}\right) + \frac{\tau}{\beta} S_\beta\left(\mathbf{x}, t^{k+1}\right) \\ &- \frac{\tau}{2nh^2}\sum_{i=1}^{n}\left[S_\beta(\mathbf{x} - h\mathbf{e}_i, t) + S_\beta(\mathbf{x} + h\mathbf{e}_i, t)\right].\end{aligned} \tag{IV.18}$$

Finally, combining like terms gives:

$$S_\beta\left(\mathbf{x}, t^k\right) = (1 + \frac{\tau}{h^2} + \frac{\tau}{\beta}) S_\beta\left(\mathbf{x}, t^{k+1}\right) - \frac{\tau}{2nh^2}\sum_{i=1}^{n}\left[S_\beta\left(\mathbf{x} - \mathbf{e}_i, t^{k+1}\right) + S_\beta\left(\mathbf{x} + \mathbf{e}_i, t^{k+1}\right)\right]. \tag{IV.19}$$

While the explicit time step yields a faster iteration, the time step must be very small to avoid instability. The implicit iteration requires solving a system of equations at each iteration but is stable if a time step $\tau$ is chosen that is on the order of $h^2$.

## IV.4 Discretization of Moment BVPs

Recall (IV.5):

$$-kU_{k-1,\beta}(\mathbf{x}) - \frac{1}{2n}\Delta U_{k,\beta}(\mathbf{x}) + \frac{1}{\beta}U_{k,\beta}(\mathbf{x}) = 0 \ \ \forall \mathbf{x} \in I,$$
$$U_{1,\beta}(\mathbf{x}) = \beta \ \ \forall \mathbf{x} \in \partial I. \tag{IV.20}$$

where $U_{k,\beta}(\mathbf{x})$ is the $k$th moment of the survival function of a particle whose natural lifetime follows the exponential distribution with expected value $\beta$. $I$ is the image that contains the shape $\bar{\Omega}$

Also recall the definition of the Laplace operator:

$$\Delta U_{k,\beta}(\mathbf{x}) = \sum_{i=1}^{n} \frac{\partial^2}{\partial x_i^2} U_{k,\beta}(\mathbf{x}) \,. \tag{IV.21}$$

Implementing the centered difference approximation of the second derivative in (IV.21) gives:

$$\begin{aligned}\Delta U_{k,\beta}(\mathbf{x}) &= \frac{1}{h^2}\sum_{i=1}^{n}\Big[U_{k,\beta}(\mathbf{x}-h\mathbf{e}_i) - 2U_{k,\beta}(\mathbf{x}) + U_{k,\beta}(\mathbf{x}+h\mathbf{e}_i)\Big]\,, \\ &= -\frac{2n}{h^2}U_{k,\beta}(\mathbf{x}) + \frac{1}{h^2}\sum_{i=1}^{n}\Big[U_{k,\beta}(\mathbf{x}-h\mathbf{e}_i) + U_{k,\beta}(\mathbf{x}+h\mathbf{e}_i)\Big]\,.\end{aligned} \tag{IV.22}$$

Substituting into (IV.5) gives:

$$-kU_{k-1,\beta}(\mathbf{x}) - \frac{1}{2n}\left[-\frac{2n}{h^2}U_{k,\beta}(\mathbf{x}) + \frac{1}{h^2}\sum_{i=1}^{n}\Big[U_{k,\beta}(\mathbf{x}-h\mathbf{e}_i) + U_{k,\beta}(\mathbf{x}+h\mathbf{e}_i)\Big]\right] + \frac{1}{\beta}U_{k,\beta}(\mathbf{x}) = 0, \tag{IV.23}$$

or,

$$-kU_{k-1,\beta}(\mathbf{x}) + \frac{1}{h^2}U_{k,\beta}(\mathbf{x}) - \frac{1}{2nh^2}\sum_{i=1}^{n}\Big[U_{k,\beta}(\mathbf{x}-h\mathbf{e}_i) + U_{k,\beta}(\mathbf{x}+h\mathbf{e}_i)\Big] + \frac{1}{\beta}U_{k,\beta}(\mathbf{x}) = 0. \tag{IV.24}$$

Combining like terms yields:

$$-kU_{k-1,\beta}(\mathbf{x}) + \left(\frac{1}{h^2}+\frac{1}{\beta}\right)U_{k,\beta}(\mathbf{x}) - \frac{1}{2nh^2}\sum_{i=1}^{n}\Big[U_{k,\beta}(\mathbf{x}-h\mathbf{e}_i) + U_{k,\beta}(\mathbf{x}+h\mathbf{e}_i)\Big] = 0. \tag{IV.25}$$

It follows that we can find the discretization of the mean, variance and higher order moments by substituting values of $k = 1, 2, 3, \ldots$. Substituting $k = 1$ into (IV.25) yields the discretization of the first moment, or mean, $U_{1,\beta}(\mathbf{x})$:

$$-U_{0,\beta}(\mathbf{x}) + \left(\frac{1}{h^2}+\frac{1}{\beta}\right)U_{1,\beta}(\mathbf{x}) - \frac{1}{2nh^2}\sum_{i=1}^{n}\left[U_{1,\beta}(\mathbf{x}-h\mathbf{e}_i) + U_{1,\beta}(\mathbf{x}+h\mathbf{e}_i)\right] = 0.$$

$U_{0,\beta}(x)$ is the zeroth moment of the survival function, which is equal to 1. So we have:

$$-1 + \left(\frac{1}{h^2} + \frac{1}{\beta}\right) U_{1,\beta}(\mathbf{x}) - \frac{1}{2nh^2} \sum_{i=1}^{n} \left[U_{1,\beta}(\mathbf{x} - h\mathbf{e}_i) + U_{1,\beta}(\mathbf{x} + h\mathbf{e}_i)\right] = 0,$$

or,

$$\left(\frac{1}{h^2} + \frac{1}{\beta}\right) U_{1,\beta}(\mathbf{x}) - \frac{1}{2nh^2} \sum_{i=1}^{n} \left[U_{1,\beta}(\mathbf{x} - h\mathbf{e}_i) + U_{1,\beta}(\mathbf{x} + h\mathbf{e}_i)\right] = 1. \tag{IV.26}$$

With the addition of the boundary conditions, (IV.26) becomes:

$$\left(\frac{1}{h^2} + \frac{1}{\beta}\right) U_{1,\beta}(\mathbf{x}) - \frac{1}{2nh^2} \sum_{i=1}^{n} \left[U_{1,\beta}(\mathbf{x} - \mathbf{e}_i) + U_{1,\beta}(\mathbf{x} + \mathbf{e}_i)\right] = 1 \ \ \forall \mathbf{x} \in \mathbb{R}^n \backslash \partial\Omega,$$

$$U_{1,\beta}(\mathbf{x}) = \beta \ \ \forall \mathbf{x} \in \partial\Omega. \tag{IV.27}$$

Substituting $k = 2$ into (IV.25) yields the discretization of the second moment of $T$.

$$-U_{1,\beta}(\mathbf{x}) + \left(\frac{1}{h^2} + \frac{1}{\beta}\right) U_{2,\beta}(\mathbf{x}) - \frac{1}{2nh^2} \sum_{i=1}^{n} \left[U_{2,\beta}(\mathbf{x} - h\mathbf{e}_i) + U_{2,\beta}(\mathbf{x} + h\mathbf{e}_i)\right] = 0, \tag{IV.28}$$

or,

$$\left(\frac{1}{h^2} + \frac{1}{\beta}\right) U_{2,\beta}(\mathbf{x}) - \frac{1}{2nh^2} \sum_{i=1}^{n} \left[U_{2,\beta}(\mathbf{x} - h\mathbf{e}_i) + U_{2,\beta}(\mathbf{x} + h\mathbf{e}_i)\right] = U_{1,\beta}(\mathbf{x}). \tag{IV.29}$$

In the following sections we explore the results obtained by solving (IV.5) on a collection of shapes. We show analytical solutions on spheres and numerical solutions on other more complicated shapes.

## IV.5 Analytical Examples

In this section we show a special case of the mean hitting time and the analytical solution on a circle or sphere of $n$-dimensions.

As shown in Appendix A.2.3, the first moment of the mean survival function of $T$ given that $\partial\Omega$ is a circle of radius $R$ is $U_{1,\beta}(r) = Y_{1,\beta}(\|\mathbf{x}\|)$, where:

$$Y_{1,\beta}(r) = \beta - \frac{\beta}{I_0\left(\frac{2R}{\sqrt{\beta}}\right)} I_0\left(\frac{2r}{\sqrt{\beta}}\right) \qquad r < R, \tag{IV.30}$$

$$Y_{1,\beta}(r) = \beta - \frac{\beta}{K_0\left(\frac{2R}{\sqrt{\beta}}\right)} K_0\left(\frac{2r}{\sqrt{\beta}}\right) \qquad R < r. \tag{IV.31}$$

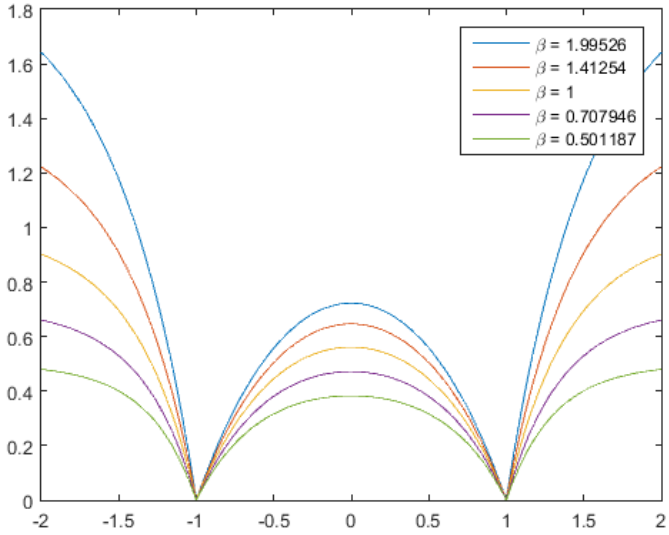


**Figure 17:** $Y_{1,\beta}$ for varying values of $\beta$ on a circle of radius $R = 1$.

$I_0$ is a modified Bessel function of the first kind and $K_0$ is a modified Bessel function of the second kind. Plots of (IV.30) and (IV.31) are shown in Figure 17 for several values of $\beta$.

## IV.6 Computational Examples of Mean Hitting Time

In this section, $U_1(\mathbf{x})$ and $U_{1,\beta}(\mathbf{x})$ are computed for various shapes. Figures 18, 20 and 22 show the shape silhouettes, mean hitting times as in Section III.3, mean dying times as in Section IV.2 and the logarithms of mean dying times.

Figures 19, 21 and 23 show the log mean dying time, $\log\left[U_{1,\beta}(\mathbf{x})\right]$, for various values of $\beta$ on a horse silhouette, a circle and a triangle with noisy boundaries, respectively. As $\beta$ increases, the intensity of $U_{1,\beta}(\mathbf{x})$ increases.

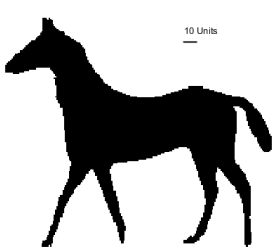


**(a)** Horse Silhouette

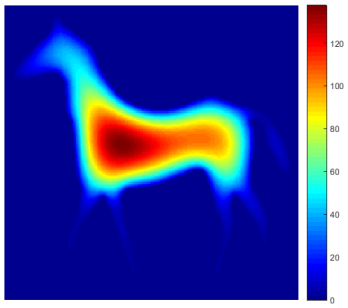


**(b)** Mean Hitting Time $U_1(\mathbf{x})$

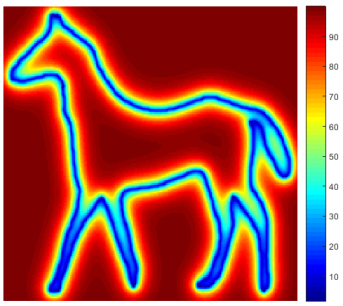


**(c)** $U_{1,\beta}(\mathbf{x})$ where $\beta = 100$

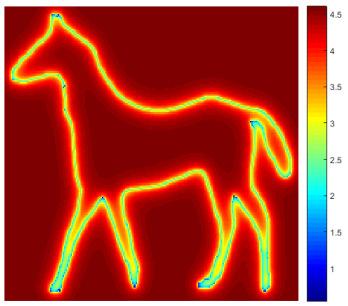


**(d)** $\log[U_{1,\beta}(\mathbf{x})]$ where $\beta = 100$

**Figure 18:** Mean hitting time $U_1(\mathbf{x})$ and mean dying time, $U_{1,\beta}(\mathbf{x})$, for points $\mathbf{x}$ both inside and outside the boundary of the shape $I$.

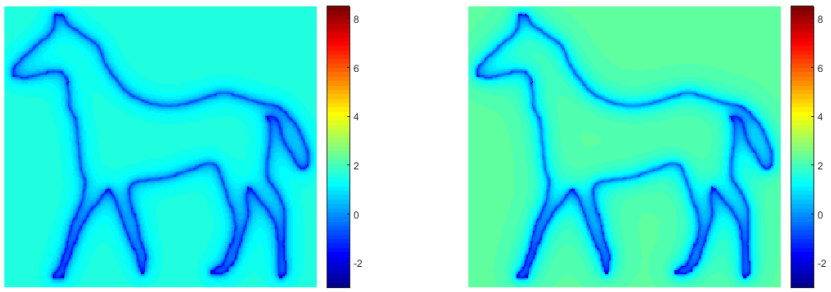

**(a)** $\beta = 5$ **(b)** $\beta = 10$

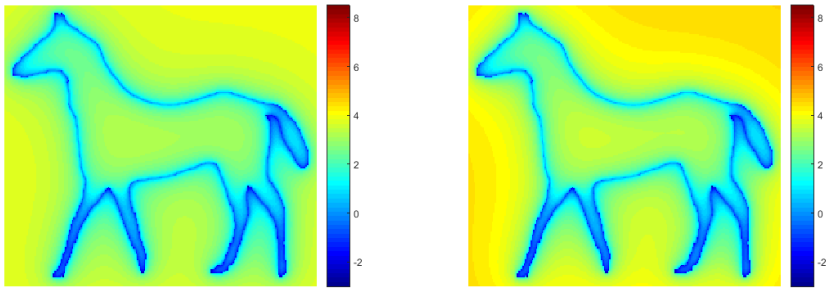

**(c)** $\beta = 50$ **(d)** $\beta = 100$

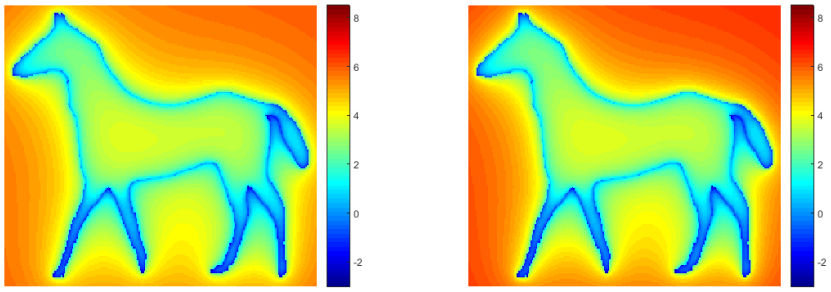

**(e)** $\beta = 500$ **(f)** $\beta = 1000$

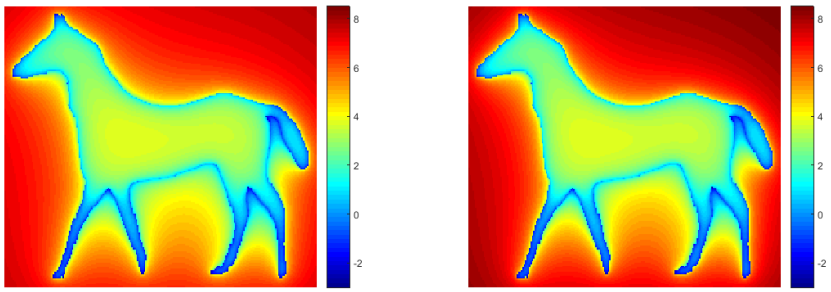

**(g)** $\beta = 5000$ **(h)** $\beta = 10000$

**Figure 19:** Log mean dying time, $\log\left[U_{1,\beta}(\mathbf{x})\right]$, for various values of $\beta$.

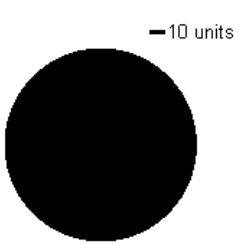


**(a)** Circle Silhouette

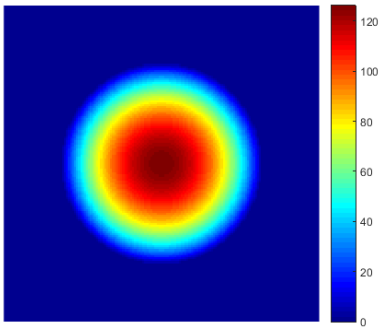


**(b)** Mean Hitting Time

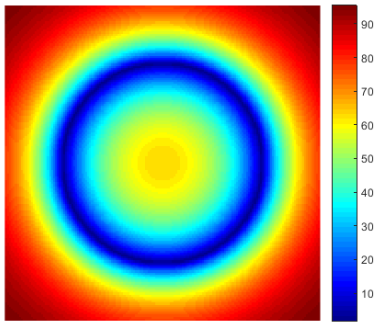


**(c)** $U_{1,\beta}(\mathbf{x})$ where $\beta = 100$

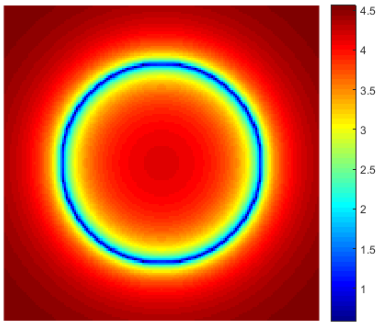


**(d)** $\log[U_{1,\beta}(\mathbf{x})]$ where $\beta = 100$

**Figure 20:** Mean dying time, $U_{1,\beta}(\mathbf{x})$, for points $\mathbf{x}$ both inside and outside the boundary of the shape $I$.

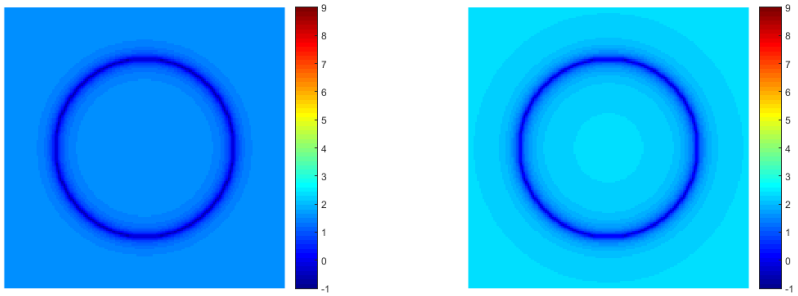

**(a)** $\beta = 5$ **(b)** $\beta = 10$

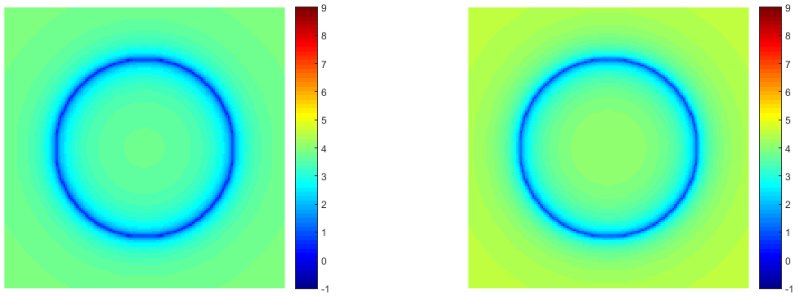

**(c)** $\beta = 50$ **(d)** $\beta = 100$

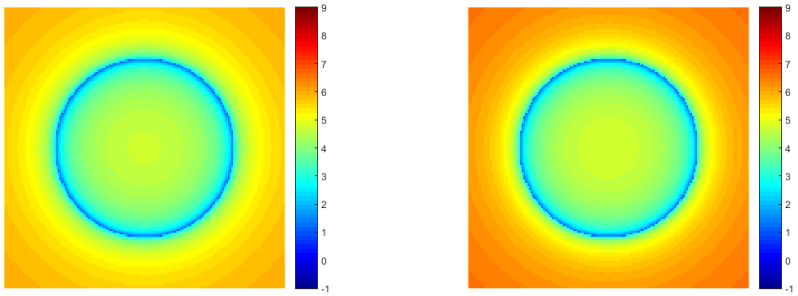

**(e)** $\beta = 500$ **(f)** $\beta = 1,000$

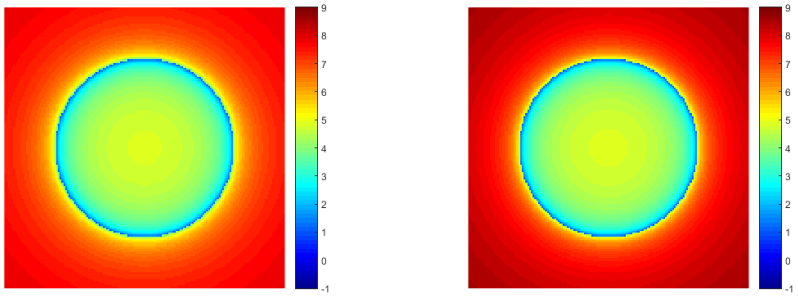

**(g)** $\beta = 5,000$ **(h)** $\beta = 10,000$

**Figure 21:** Log mean dying time, $\log\left[U_{1,\beta}(\mathbf{x})\right]$, for varying values of $\beta$.

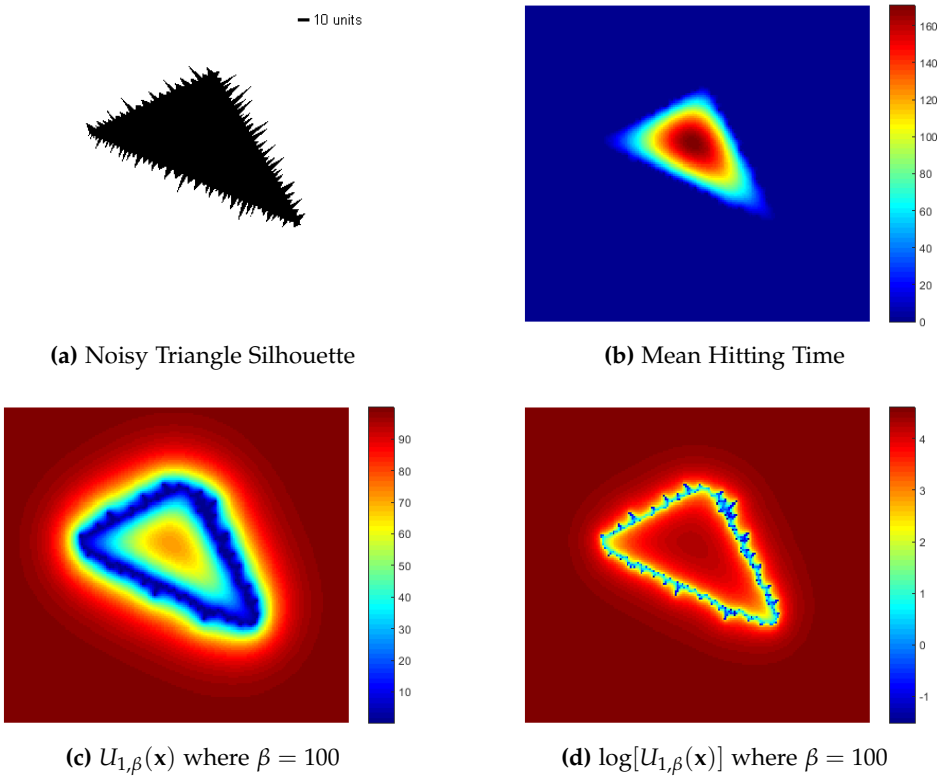


**(a)** Noisy Triangle Silhouette

**(b)** Mean Hitting Time

**(c)** $U_{1,\beta}(\mathbf{x})$ where $\beta = 100$

**(d)** $\log[U_{1,\beta}(\mathbf{x})]$ where $\beta = 100$

**Figure 22:** Mean dying time, $U_{1,\beta}(\mathbf{x})$, for points $\mathbf{x}$ both inside and outside the boundary of the shape $I$.

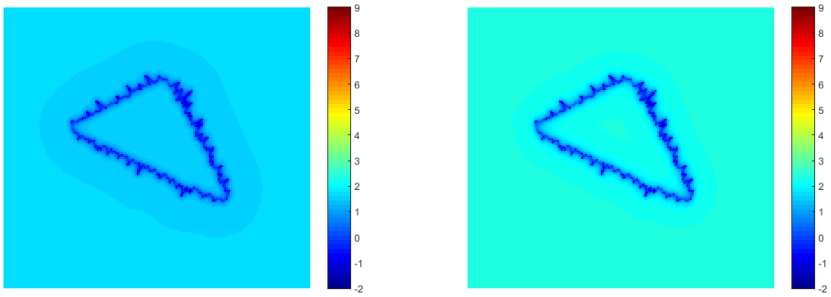

**(a)** $\beta = 5$ **(b)** $\beta = 10$

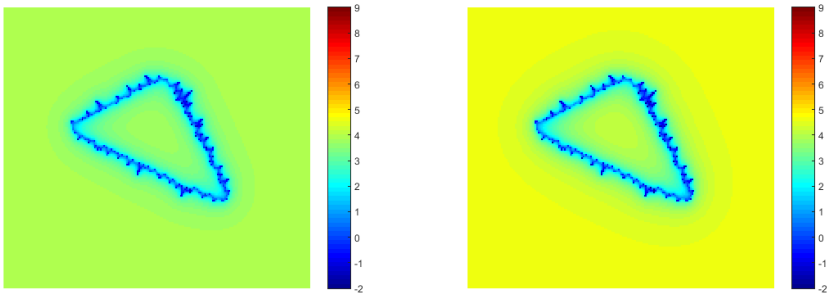

**(c)** $\beta = 50$ **(d)** $\beta = 100$

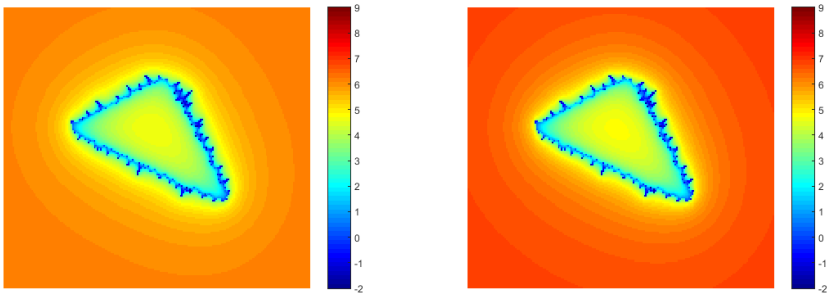

**(e)** $\beta = 500$ **(f)** $\beta = 1,000$

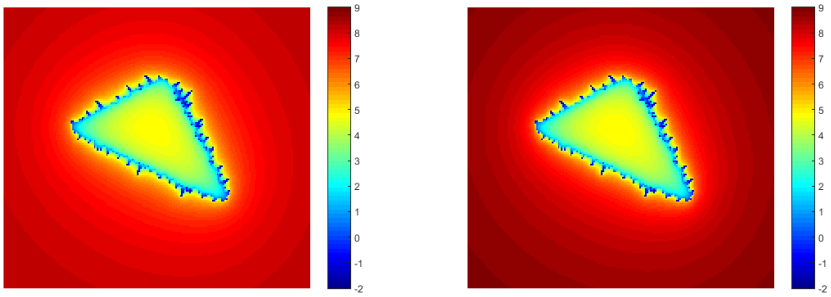

**(g)** $\beta = 5,000$ **(h)** $\beta = 10,000$

**Figure 23:** Log mean dying time, $\log\left[U_{1,\beta}(\mathbf{x})\right]$, for varying values of $\beta$.

## IV.7 Computational Examples of Moments

In this section, we compute the dying time and higher moments defined in Section IV.2 for various silhouette images.

The standardized moments of the dying time, $W_{k,\beta}(\mathbf{x})$, are shown in Figures 24, 27 and 30 for a horse, circle and triangle silhouette, respectively. Figures 25, 28 and 31 show the moments about zero $U_{k,\beta}(\mathbf{x})$. The central moments $V_{k,\beta}(\mathbf{x})$ are shown in Figures 26, 29, and 32 .

Similar to the hitting time moments in Section III.3, the level sets of $U_{k,\beta}(\mathbf{x})$, $V_{k,\beta}(\mathbf{x})$ and $W_{k,\beta}(\mathbf{x})$ are smoothed versions of the bounding contour. Inside the shape, the maximum values are achieved near the centroid, and outside the shape the maximum values are near the image boundary for the moments about zero, $U_{k,\beta}(\mathbf{x})$, the central moments, $V_{k,\beta}(\mathbf{x})$, and the standard deviation $W_{2,\beta}(\mathbf{x})$. The skewness, $W_{3,\beta}(\mathbf{x})$, and kurtosis $W_{4,\beta}(\mathbf{x})$ achieve maximum values near the shape boundary.

As in Section III.3, the skewness and kurtosis values are noisy on the boundaries of the shape and using the reciprocals of the skewness and kurtosis, $\frac{1}{W_{3,\beta}(\mathbf{x})}$ and $\frac{1}{W_{4,\beta}(\mathbf{x})}$, provides a better visualization.

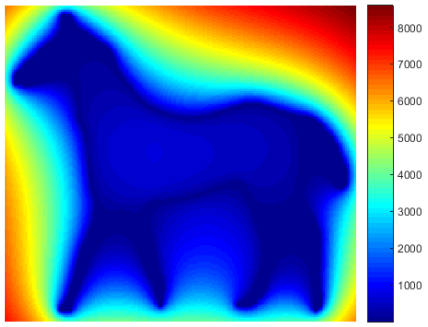


Variance

$V_{2,100}(\mathbf{x})$

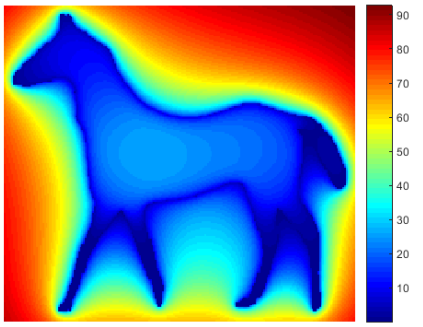


Standard Deviation

$W_{2,100}(\mathbf{x})$

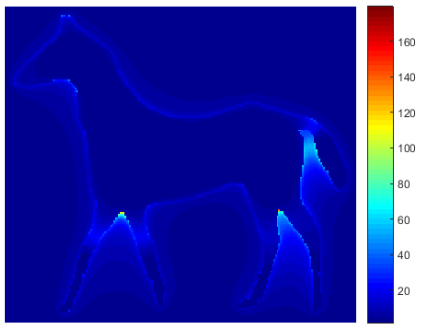


Skewness

$W_{3,100}(\mathbf{x})$

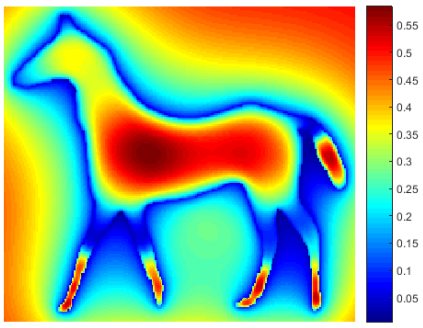


Reciprocal of Skewness

$\frac{1}{W_{3,100}(\mathbf{x})}$

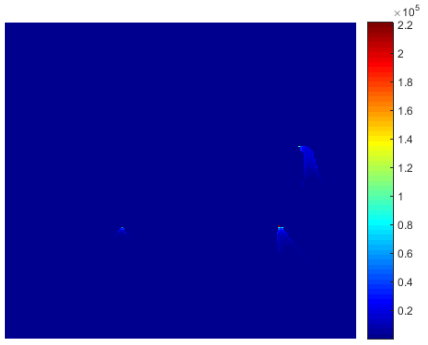


Kurtosis

$W_{4,100}(\mathbf{x})$

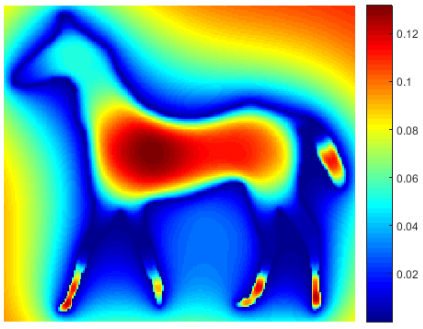


Reciprocal of Kurtosis

$\frac{1}{W_{4,100}(\mathbf{x})}$

**Figure 24:** Moments of $T$.

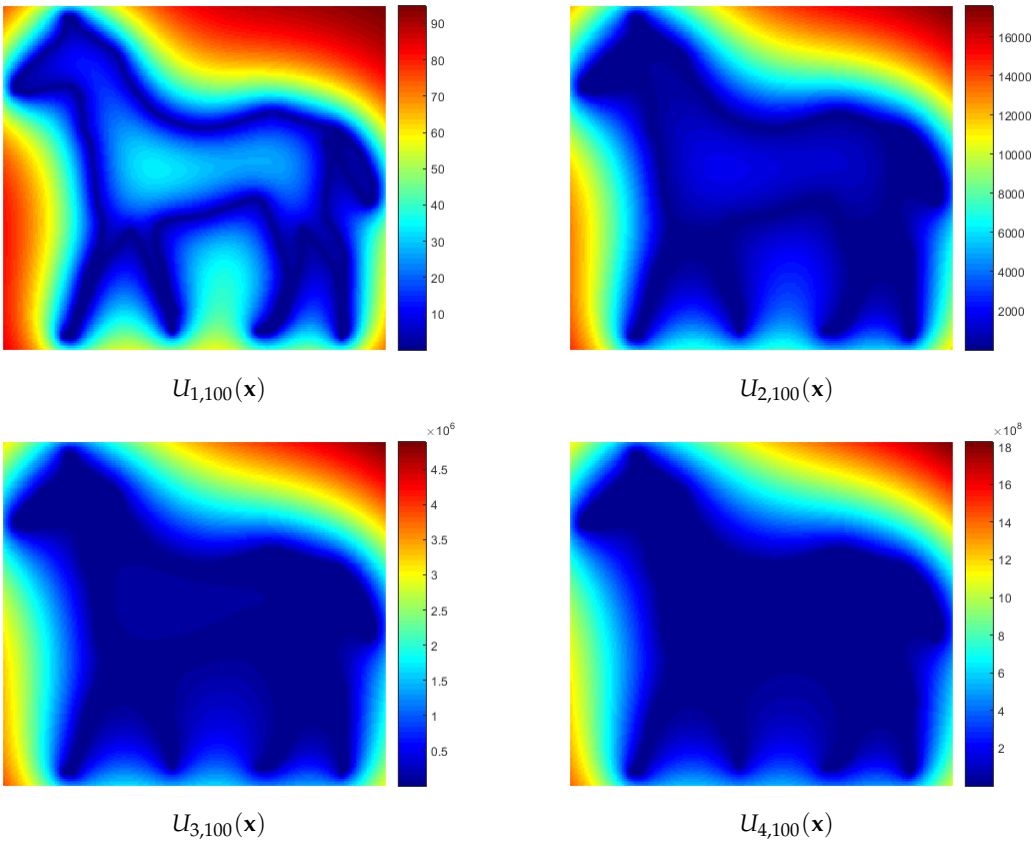


$U_{1,100}(\mathbf{x})$ $U_{2,100}(\mathbf{x})$

$U_{3,100}(\mathbf{x})$ $U_{4,100}(\mathbf{x})$

**Figure 25:** $k^{th}$ Moments About Zero of $T$.

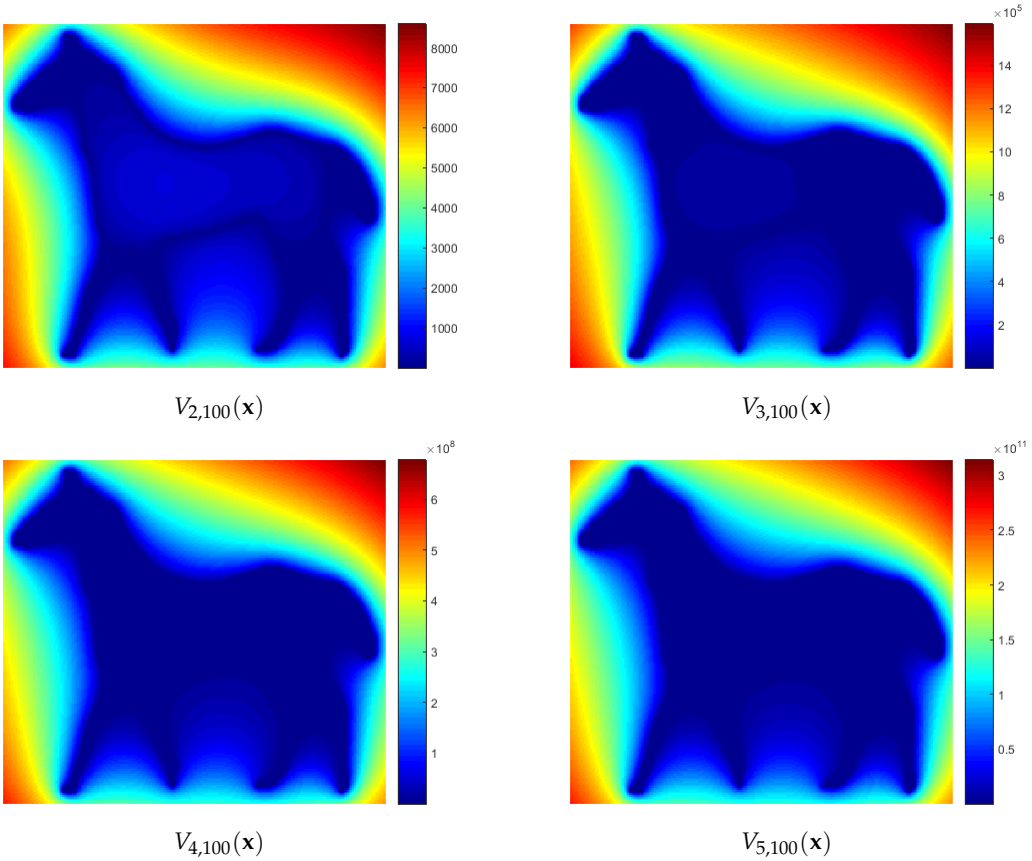


$V_{2,100}(\mathbf{x})$ $V_{3,100}(\mathbf{x})$

$V_{4,100}(\mathbf{x})$ $V_{5,100}(\mathbf{x})$

**Figure 26:** $k^{th}$ Central Moments of $T$.

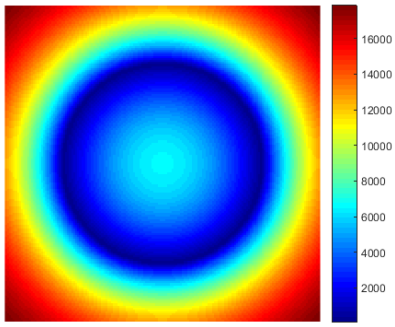


Variance

$V_{2,100}(\mathbf{x})$

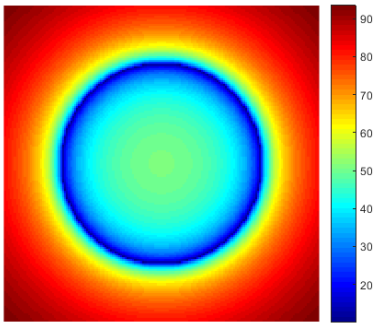


Standard Deviation

$W_{2,100}(\mathbf{x})$

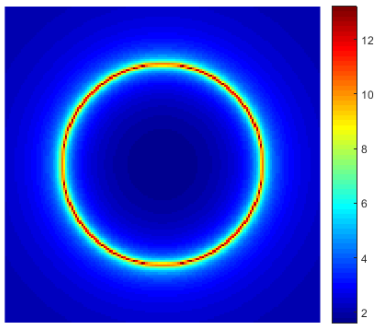


Skewness

$W_{3,100}(\mathbf{x})$

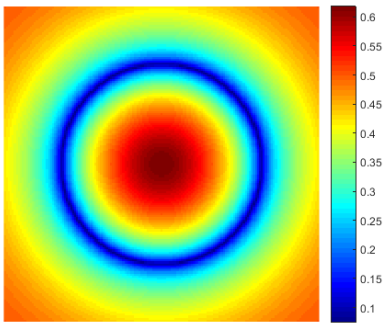


Reciprocal of Skewness

$\frac{1}{W_{3,100}(\mathbf{x})}$

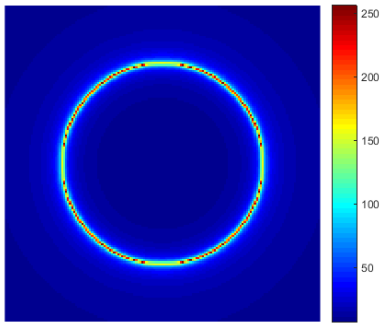


Kurtosis

$W_{4,100}(\mathbf{x})$

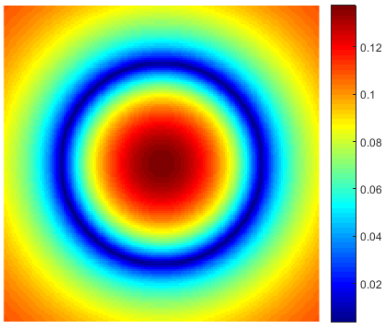


Reciprocal of Kurtosis

$\frac{1}{W_{4,100}(\mathbf{x})}$

**Figure 27:** Moments of $T$.

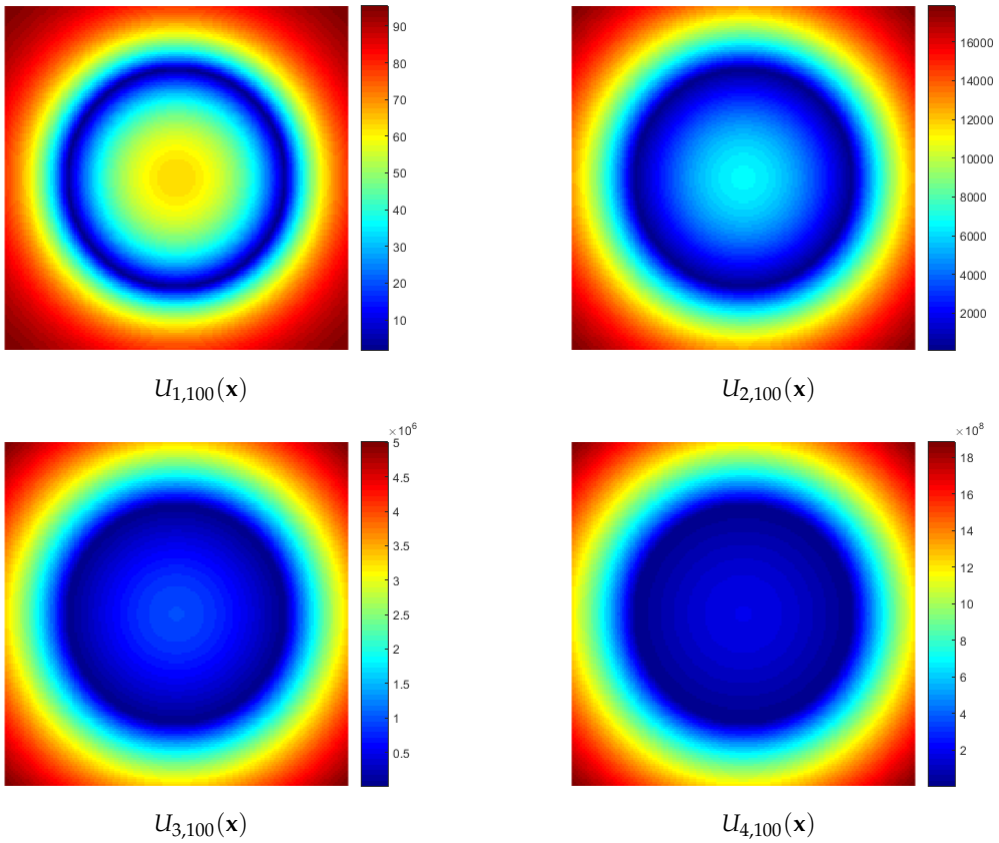


$U_{1,100}(\mathbf{x})$ $U_{2,100}(\mathbf{x})$

$U_{3,100}(\mathbf{x})$ $U_{4,100}(\mathbf{x})$

**Figure 28:** $k^{th}$ Moments About Zero of $T$.

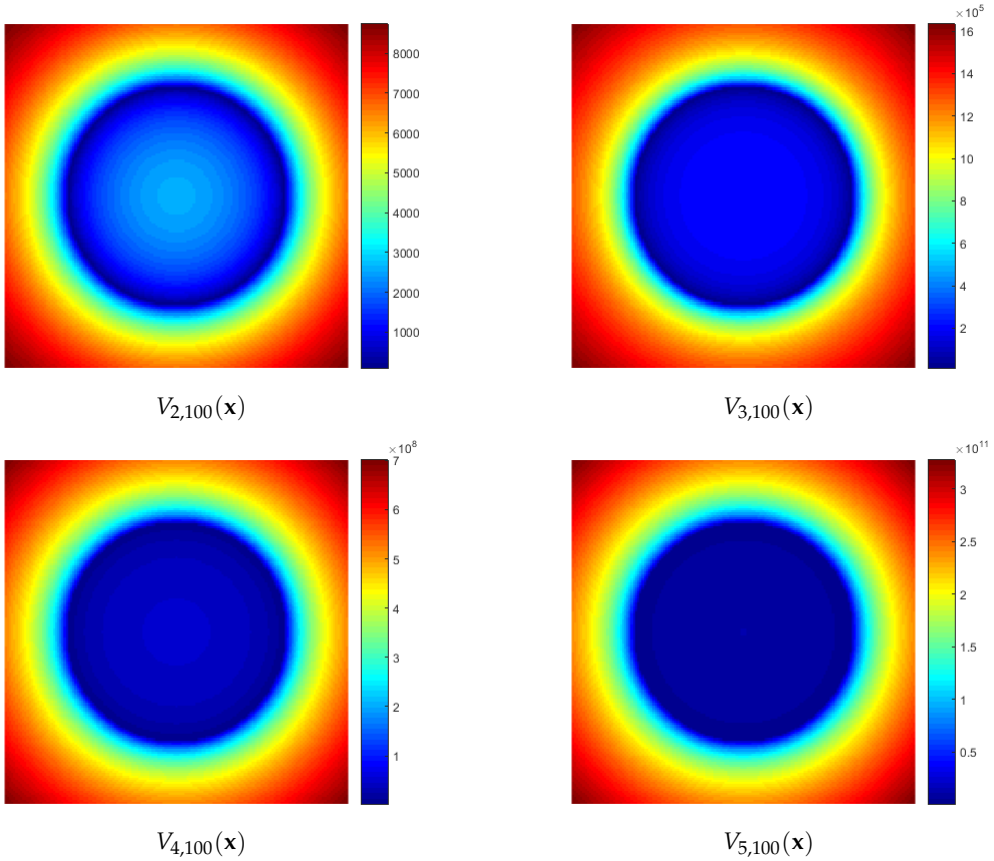


$V_{2,100}(\mathbf{x})$ $V_{3,100}(\mathbf{x})$

$V_{4,100}(\mathbf{x})$ $V_{5,100}(\mathbf{x})$

**Figure 29:** $k^{th}$ Central Moments of $T$.

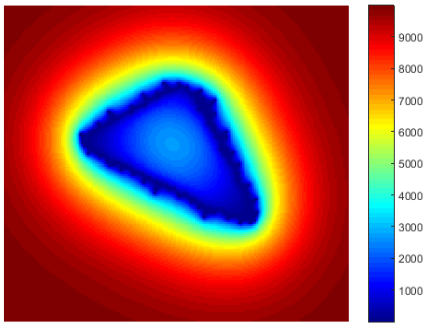


Variance

$V_{2,100}(\mathbf{x})$

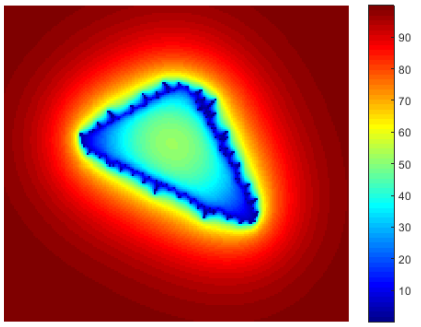


Standard Deviation

$W_{2,100}(\mathbf{x})$

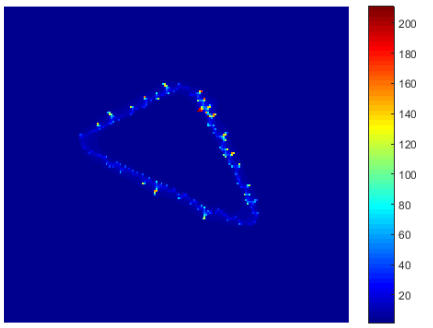


Skewness

$W_{3,100}(\mathbf{x})$

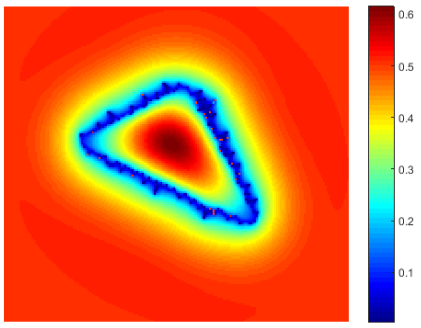


Reciprocal of Skewness

$\frac{1}{W_{3,100}(\mathbf{x})}$

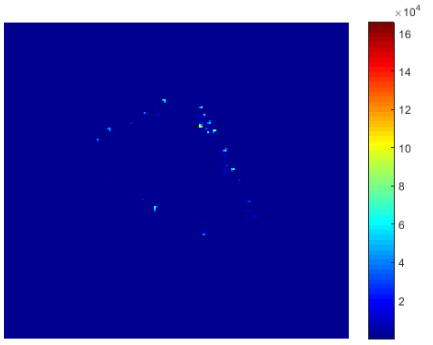


Kurtosis

$W_{4,100}(\mathbf{x})$

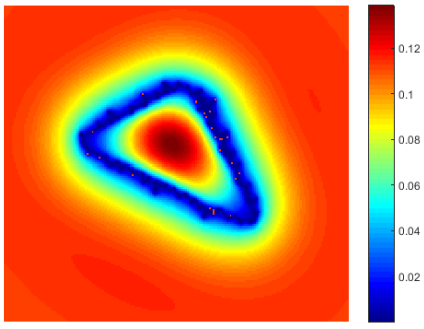


Reciprocal of Kurtosis

$\frac{1}{W_{4,100}(\mathbf{x})}$

**Figure 30:** Moments of $T$.

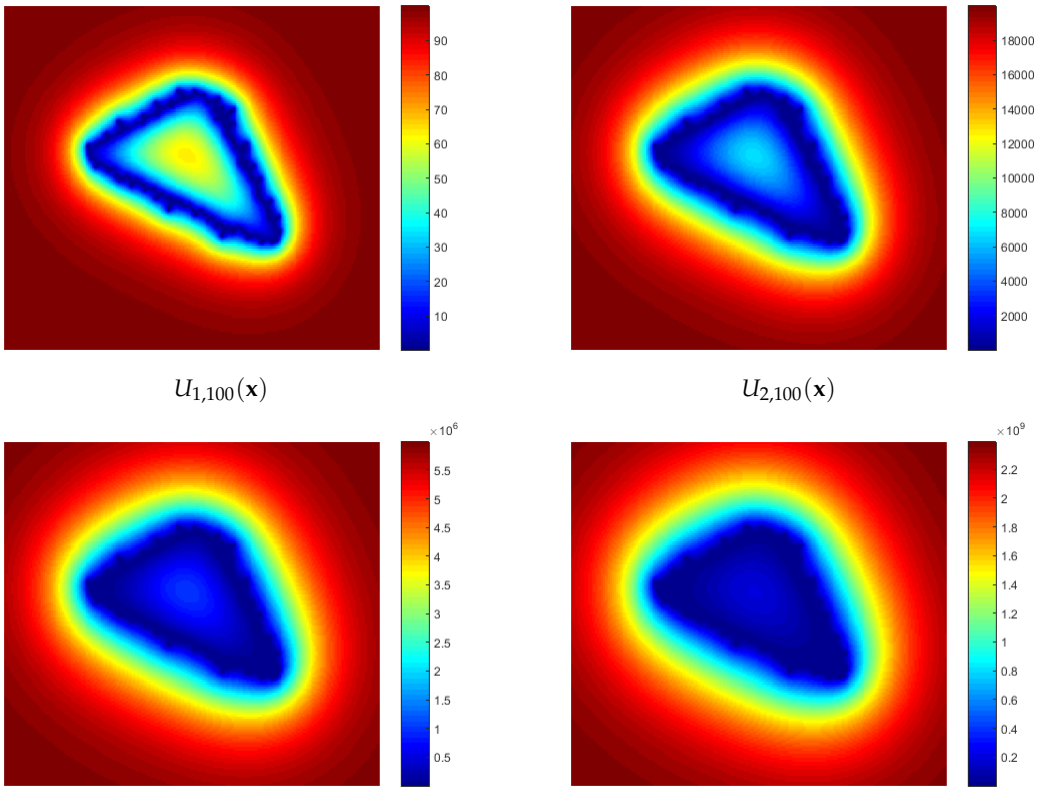


**Figure 31:** $k^{th}$ Moments About Zero of $T$.

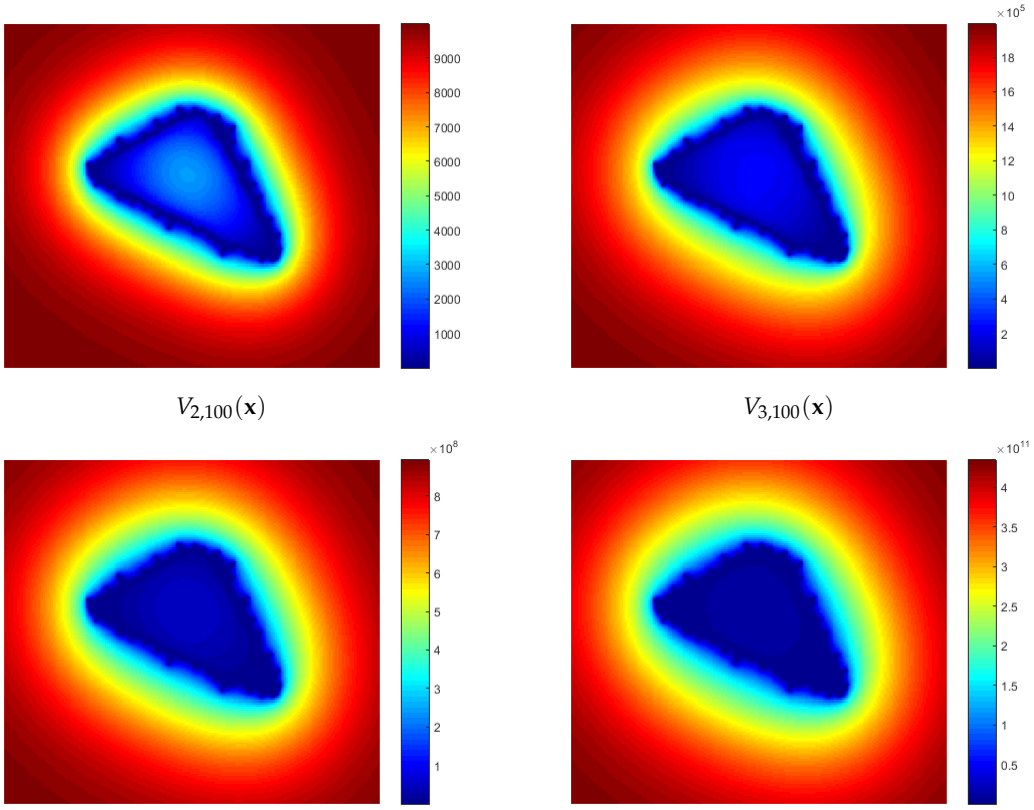


$V_{2,100}(\mathbf{x})$ $V_{3,100}(\mathbf{x})$

$V_{4,100}(\mathbf{x})$ $V_{5,100}(\mathbf{x})$

**Figure 32:** $k^{th}$ Central Moments of $T$.

# V. Classification Experiments

In order to determine the efficacy of utilizing the features presented in Section IV.7, we perform classification experiments using two datasets. The data, experiments, and results are described in the following sections.

## V.1 Data

We present results using two publicly available datasets.

The first is a collection of natural silhouettes. There are 12 classes of images (cups, hands, humans, horses, birds, fish, rays, cats, dogs and elephants), with 490 images total, and Figure 33 shows examples from each class of silhouettes. This particular collection of silhouettes was first used in [14].

The second dataset is the MNIST database of handwritten digits [16], with a training set of 60,000 examples and a test set of 10,000 examples.

## V.2 Experimental Setup

To determine the efficacy of utilizing the dying time moments presented in Section IV.2 in shape classification, we use support vector machines, or SVMs, to classify images based on the proposed features. The classification is performed using a multiclass SVM with a one-versus-all method, as implemented in MATLAB, with 20% of the images used as training data for the natural silhouettes dataset, and 86% used to train the classifier for the MNIST handwritten digit database.

The shape descriptors used were mean, standard deviation, skewness, and kurtosis, as described in Sections III.2 and IV.2. These were computed for each image using both the hitting time and the dying time. When using the hitting time shape descriptor, the values were computed inside the shape. When using the dying time, the values were computed both inside and outside the shape.

## V.3 Results

We quantified the results using confusion matrices, which indicate the number of true positives (TP), false positives (FP), false negatives (FN) and true negatives (TN) from each experiment. The

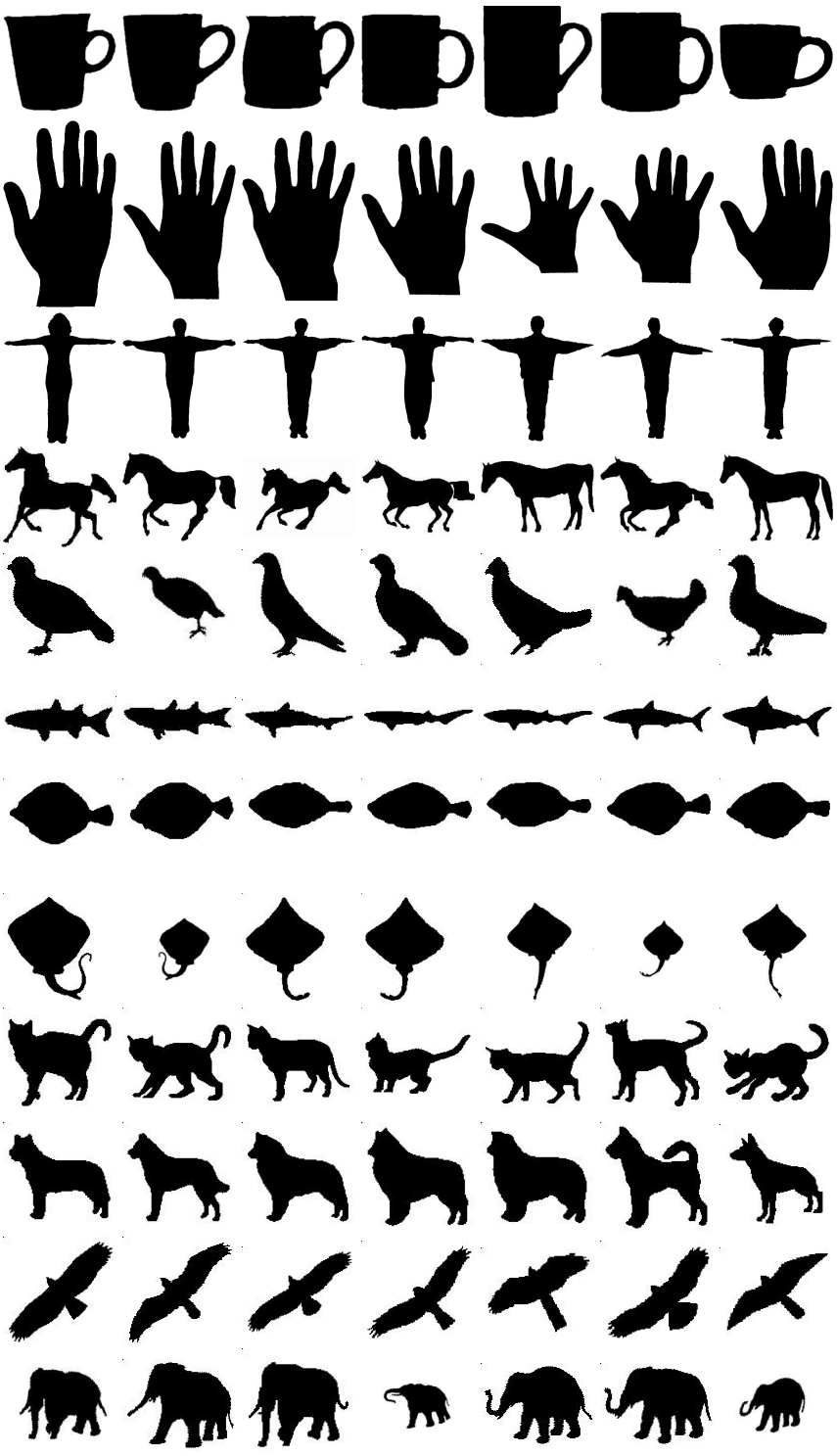

**Figure 33:** Sample images from natural silhouettes dataset.

**Figure 34:** Sample images from MNIST database.

performance measures derived from each confusion matrix are as follows:

accuracy (A):

$$A = \frac{TP + TN}{TP + TN + FP + FN}, \tag{V.1}$$

precision (P):

$$P = \frac{TP}{TP + FP}, \tag{V.2}$$

sensitivity (Se):

$$Se = \frac{TP}{TP + FN}, \tag{V.3}$$

and specificity (Sp):

$$Sp = \frac{TN}{FP + TN}. \tag{V.4}$$

We performed the classification four different ways. First, we used the hitting time from Chapter III inside the shape. Second, we used the dying time from Chapter IV both inside and outside the shape. Third, with dying time just outside the shape. Finally, we performed the classification with the hitting time moments inside the shape and dying time moments outside the shape fused together.

Tables 1 and 2 show the natural silhouette and handwritten digit classification experiment results, respectively. The average accuracy (AA), average precision (AP), average sensitivity (ASe) and average specificity (ASp) are shown in the first four rows for each set of features: hitting time

inside the shape (HT), dying time inside and outside the shape (DT), dying time outside the shape only (DTOut) and the hitting time inside the shape fused with the dying time outside the shape (Fused). The remaining rows show the average accuracy for each method across all classes.

Table 1, shows the results of classification based the dying time outside the shape fused with the hitting time inside the shape outperformed the other features in accuracy, precision, sensitivity and specificity over all twelve classes of natural silhouettes. Specifically, classes 1 (mug), 4 (horse), 6 (shark), 7 (fish), 8 (stingray), 9 (cat), 10 (dog) and 12 (elephant) showed an improvement in accuracy.

As we saw with the the natural silhouettes, when classifying the handwritten digits based on the dying time outside the shape fused with the hitting time inside the shape outperformed the other features in accuracy, precision, sensitivity and specificity over all 10 classes of digits, as shown in Table 2. Specifically, numerals 0, 1, 2, 3, 4, 5, 7, 8, and 9 showed an improvement in accuracy.

| | No. of Samp | HT | DT | DTOut | Fused |
|---|---|---|---|---|---|
| Average Accuracy | - | 94.14 | 92.03 | 91.99 | **95.39** |
| Average Precision | - | 64.46 | 48.89 | 49.73 | **74.22** |
| Average Sensitivity | - | 67.39 | 49.46 | 48.76 | **72.26** |
| Average Specificity | - | 96.82 | 95.64 | 95.62 | **97.47** |
| Class 1: Mug | 26 | 98.71 | 95.09 | 96.64 | **99.22** |
| Class 2: Hand | 26 | **99.74** | 96.90 | 95.87 | 99.48 |
| Class 3: Person | 55 | 97.67 | 97.67 | **97.93** | 97.67 |
| Class 4: Horse | 80 | 83.46 | 91.21 | 91.47 | **91.73** |
| Class 5: Bird | 50 | **89.92** | 84.75 | 83.98 | 89.41 |
| Class 6: Shark | 43 | 96.64 | 94.83 | 94.57 | **96.90** |
| Class 7: Fish | 28 | 95.87 | 91.47 | 91.47 | **97.93** |
| Class 8: Stingray | 47 | 93.54 | 86.56 | 87.60 | **94.32** |
| Class 9: Cat | 42 | 89.66 | 86.30 | 85.79 | **92.51** |
| Class 10: Dog | 49 | 91.73 | 88.11 | 88.63 | **91.99** |
| Class 11: Hawk | 17 | 96.64 | 96.38 | **97.16** | 96.90 |
| Class 12: Elephant | 27 | 96.12 | 95.09 | 92.76 | **96.64** |

**Table 1:** Natural silhouettes classification results. Class rows show per-class accuracy. All quantities are percentages, with the exception of the number of samples.

| | No. of Samp | HT | DT | DTOut | Fused |
|---|---|---|---|---|---|
| Average Accuracy | - | 88.46 | 88.26 | 87.94 | **90.99** |
| Average Precision | - | 41.29 | 40.44 | 38.97 | **54.21** |
| Average Sensitivity | - | 39.29 | 37.57 | 36.53 | **52.37** |
| Average Specificity | - | 93.66 | 93.56 | 93.37 | **95.07** |
| Class 0 | 10,000 | 86.99 | 85.84 | 85.75 | **93.51** |
| Class 1 | 10,000 | 97.34 | 96.18 | 95.77 | **98.08** |
| Class 2 | 10,000 | 87.36 | 85.94 | 86.56 | **88.26** |
| Class 3 | 10,000 | 86.22 | 87.47 | 87.18 | **88.82** |
| Class 4 | 10,000 | 86.78 | 87.82 | 86.59 | **89.34** |
| Class 5 | 10,000 | 88.21 | 88.66 | 88.24 | **89.58** |
| Class 6 | 10,000 | 87.57 | **91.60** | 90.64 | 91.18 |
| Class 7 | 10,000 | 90.93 | 87.88 | 87.80 | **92.02** |
| Class 8 | 10,000 | 85.85 | 85.50 | 84.00 | **88.87** |
| Class 9 | 10,000 | 87.33 | 85.67 | 86.89 | **90.28** |

**Table 2:** Digits classification results. Class rows show per-class accuracy. All quantities are percentages, with the exception of the number of samples.

The following figures provide a visual representation of the comparison of the confusion matrices that report the classification results using the hitting time moments and the hitting time moments inside the shape fused with the dying time moments outside the shape.

Figures 35 and 36 show the true positives, or horses correctly classified as horses, from the hitting time and fused hitting time and dying time experiments, respectively. The hitting time experiment resulted in 55 true positives and the hitting time fused with dying time resulted in 52 true positives.

Figures 37 and 38 show the false positives, or non-horse images incorrectly classified as horses, from the hitting time and fused hitting time and dying time experiments, respectively. Here we see that fusing the hitting time and dying time features decreases the number of false positives by 63.6%, with 55 false positives using only the hitting time and 20 false positives with the hitting time and dying time fused.

Figures 39 and 40 show the false negatives, or horse images incorrectly classified as non-horses, from the hitting time and fused hitting time and dying time experiments, respectively. There were

9 false negatives using the hitting time features, and 12 when using the hitting time fused with dying time.

The true negatives, all other images correctly classified as non-horses, are not shown. There were 371 hitting time true negatives and 403 fused hitting time and dying time true negatives.

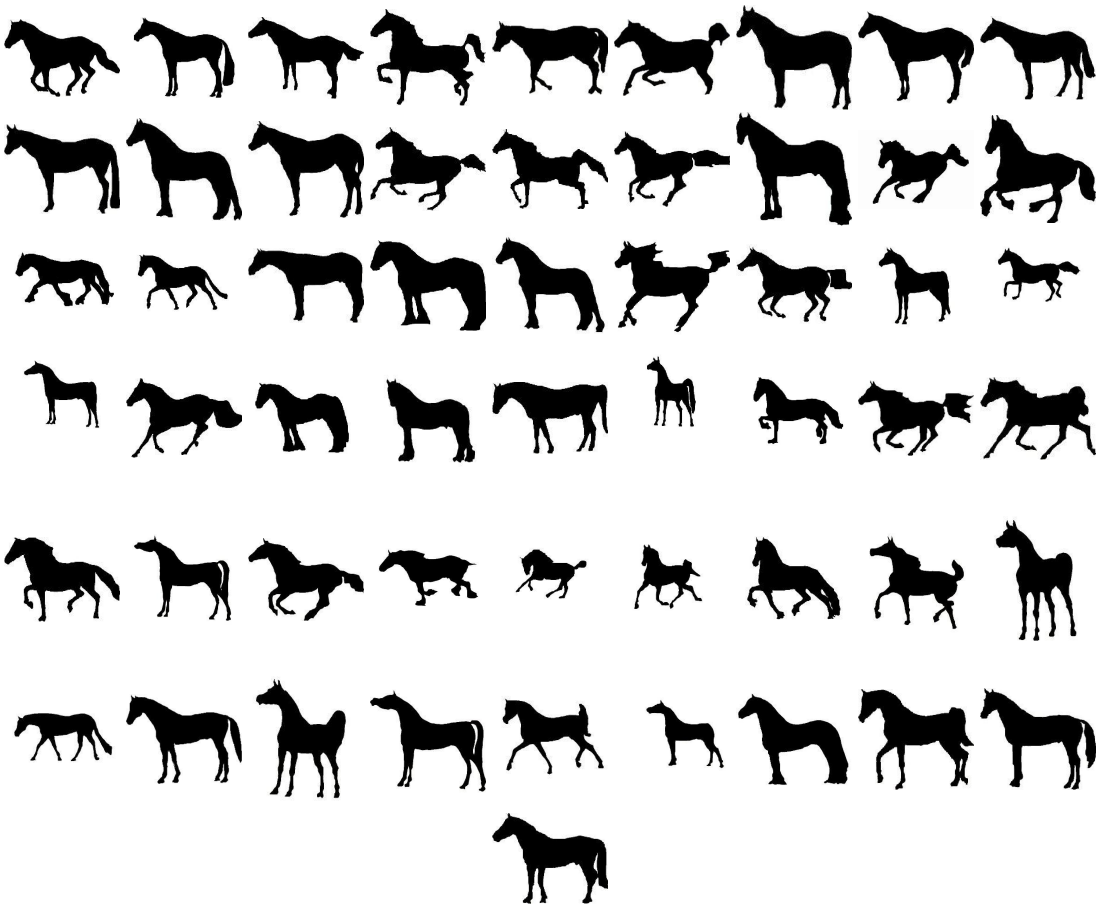

**Figure 35:** Class 4 (horse) true positives from hitting time experiment.

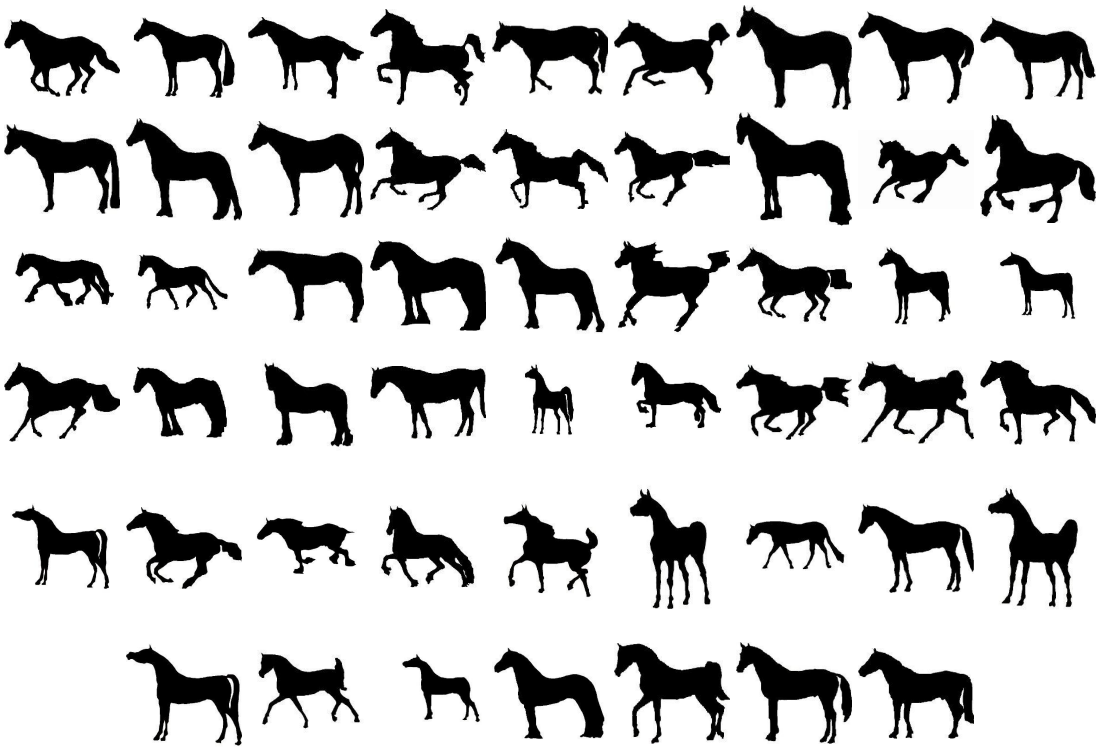

**Figure 36:** Class 4 (horse) true positives from hitting time fused with dying time experiment.

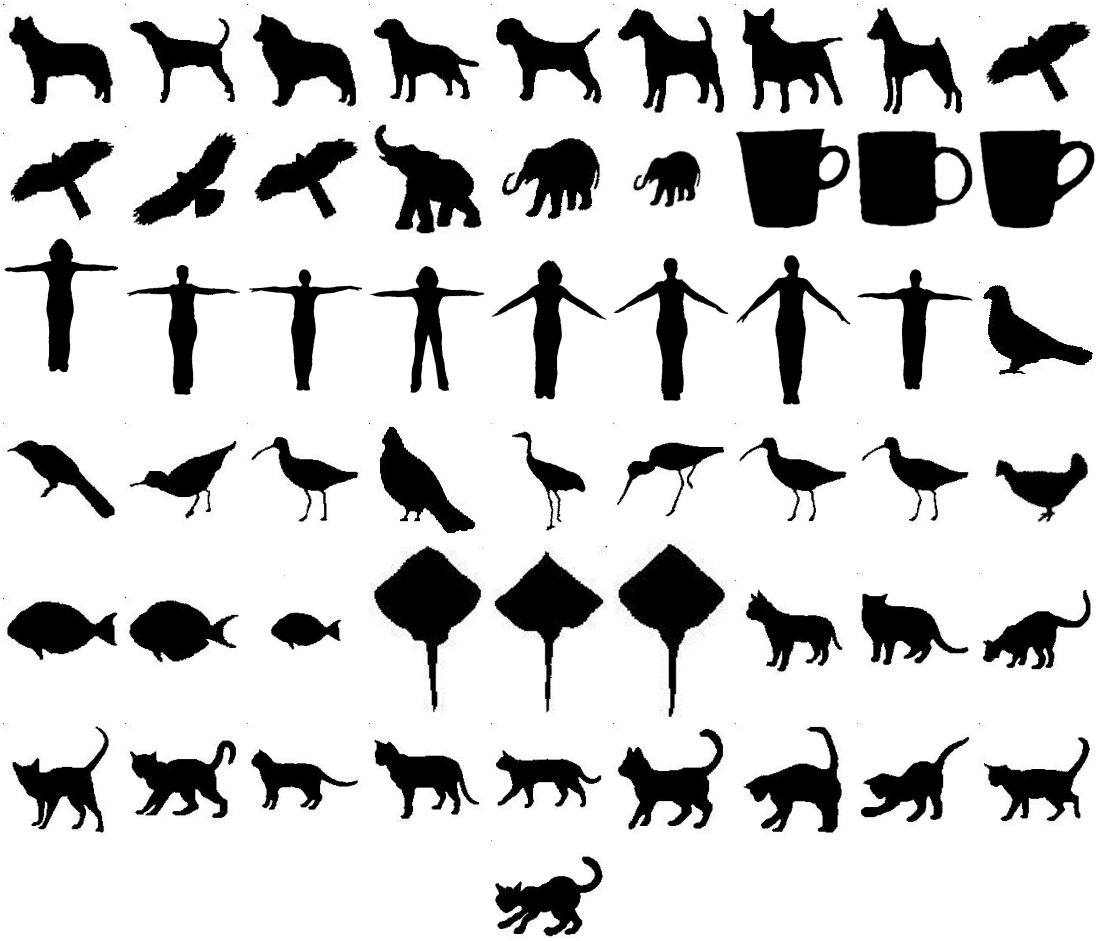

**Figure 37:** Class 4 (horse) false positives from hitting time experiment.

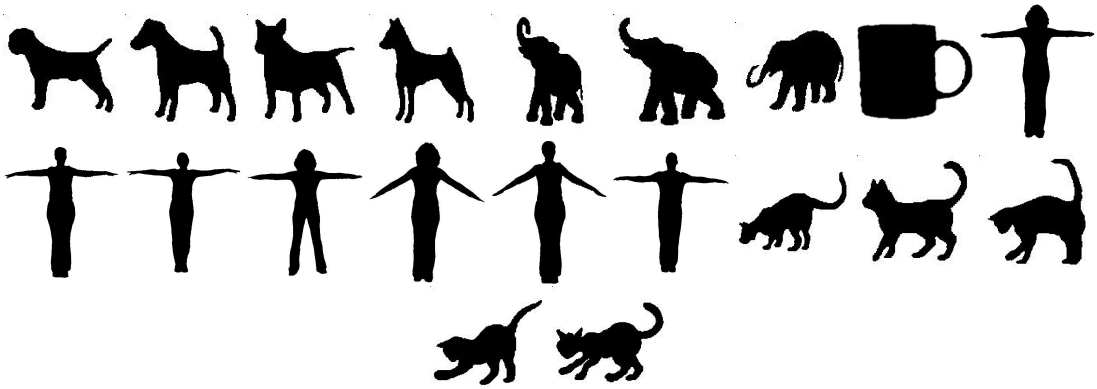

**Figure 38:** Class 4 (horse) false positives from hitting time fused with dying time experiment.

**Figure 39:** Class 4 (horse) false negatives from hitting time experiment.

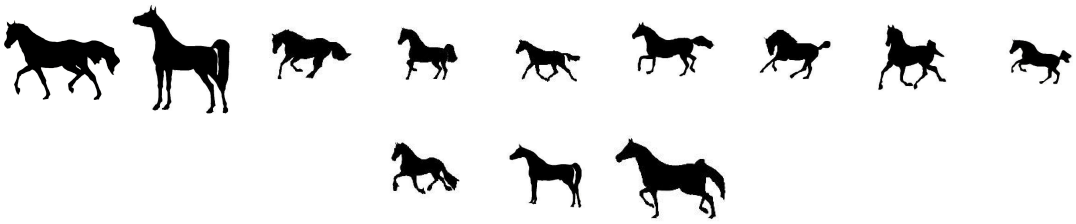

**Figure 40:** Class 4 (horse) false negatives from hitting time fused with dying time experiment.

# VI. Conclusion

Solutions to the Helmholtz equation provide meaningful information about a shape silhouette that was shown to be useful in classification. Using these features, we were able to improve an existing method of shape representation. The features extracted with this representation allowed for an improvement in the effectiveness of shape classification.

First, in Chapter III we established the survival function and its corresponding initial value problem, and showed its mean and higher order moments. We then illustrated these features computed inside various shape silhouettes.

In Chapter IV, we extended the analysis to the outside of the shape by incorporating a natural lifetime into the survival function. As before, we illustrated these features computed for silhouette images, both inside and outside the silhouette boundary.

Finally, in Chapter V we used the features developed in the preceding chapters to perform classification experiments to determine the efficacy of the new features. We performed the experiment on two databases of images, both natural shape silhouettes and handwritten numerals, and saw an increase in accuracy and decrease in the rate of false positives when using the new features computed from the survival function outside the shape in conjunction with the survival function inside the shape.

A possibility for future research is to extend this approach to higher dimensions, as we have explored only the representation and classification of shapes in two dimensions. Additionally, the Helmholtz shape classification approach could be extended to space-time action recognition, similar to the work done by Blank et al in [4].

# VII. Acknowledgments

First and foremost, I must express my sincere gratitude to my advisor Dr. Nathan Cahill, for his enthusiasm, patience and immense knowledge. His drive and dedication motivated me throughout my work. Dr. Cahill is a true mentor and his contributions were invaluable to this thesis. I am also indebted to my committee members for providing their insight and expertise. Additionally, I'd like to thank the rest of the faculty in the RIT Department of Mathematics, as well as my classmates for their continued help and inspiration.

I must also thank my friends and family for the never ending love and support they have provided. A special thanks to Adam for his understanding and for cooking me countless dinners while I worked, and to the rest of the Candela family for their continuous encouragement. Finally, thanks to Abby and my parents for always being in my corner and supporting my goals and aspirations.

# A. Appendix

## A.1 Brownian Motion Inside a Shape

### A.1.1 Hitting Time Boundary Value Problem

This appendix establishes that the survival function $S(\mathbf{x}, t)$ defined in (III.1) satisfies the IBVP given in (III.2).

Suppose $\bar{\Gamma} \subset \bar{\Omega}$ is a $n$-dimensional uniform grid of points. Each grid point $\mathbf{x}$ has neighborhood $\mathcal{N}(\mathbf{x}) = \bar{\Gamma} \cap \{\mathbf{x} \pm h\mathbf{e}_j | j = 1, \ldots, n\}$, where $\mathbf{e}_j$ is the $j^{\text{th}}$ column of the $n$-dimensional identity matrix, and $h$ is the grid spacing. The interior $\Gamma$ contains all points in $\bar{\Gamma}$ that have $2n$ neighbors (i.e., points for which $|\mathcal{N}(\mathbf{x})| = 2n$), and the discrete boundary $\partial\Gamma = \bar{\Gamma} \backslash \Gamma$.

Consider a particle that undergoes a symmetric random walk on $\bar{\Gamma}$. Let $\tau$ be the finite time between steps of the random walk. The position of the particle is given by $X(t)$, where $t$ represents continuous time; hence, $X(t)$ is piecewise constant with steps at $t = k\tau$, $k = 0, 1, 2, \ldots$. The hitting time $T_B$ corresponds to the first time the particle lands in $\partial\Gamma$; i.e. $T_B = \inf_{t \geq 0}\{t | X(t) \in \partial\Gamma\}$.

The survival function $S(\mathbf{x}, t)$ is defined as in (III.1); i.e., $S(\mathbf{x}, t) = P(T_B > t | X(0) = \mathbf{x})$. If we condition on the first step of the random walk, for points in $\Gamma$ we have:

$$\begin{aligned}
S(\mathbf{x}, t+\tau) &= \Pr\{T_B > t+\tau \,|\, X(0) = \mathbf{x}\} \\
&= \sum_{j=1}^{n} \left[ \begin{array}{l} \Pr\{T_B > t+\tau | X(0) = \mathbf{x}, X(1) = \mathbf{x} + h\mathbf{e}_j\} \Pr\{X(1) = \mathbf{x} + h\mathbf{e}_j | X(0) = \mathbf{x}\} \\ +\quad \Pr\{T_B > t+\tau | X(0) = \mathbf{x}, X(1) = \mathbf{x} - h\mathbf{e}_j\} \Pr\{X(1) = \mathbf{x} - h\mathbf{e}_j | X(0) = \mathbf{x}\} \end{array} \right] \\
&= \frac{1}{2n} \sum_{j=1}^{n} \left[ \begin{array}{l} \Pr\{T_B > t \,|\, X(0) = \mathbf{x} + h\mathbf{e}_j\} \\ \quad +\quad \Pr\{T_B > t \,|\, X(0) = \mathbf{x} - h\mathbf{e}_j\} \end{array} \right] \\
&= \frac{1}{2n} \sum_{j=1}^{n} \left[ S(\mathbf{x} + h\mathbf{e}_j, t) + S(\mathbf{x} - h\mathbf{e}_j, t) \right]. \qquad \text{(A.1)}
\end{aligned}$$

Alternatively, expanding $S(\mathbf{x}, t)$ about $t$ yields:

$$S(\mathbf{x}, t+\tau) = S(\mathbf{x}, t) + \tau \frac{\partial}{\partial t} S(\mathbf{x}, t) + O\left(\tau^2\right), \qquad \text{(A.2)}$$

and so combining (A.1) and (A.2) gives:

$$S(\mathbf{x}, t) + \tau \frac{\partial}{\partial t} S(\mathbf{x}, t) = \frac{1}{2n} \sum_{j=1}^{n} \left[ S(\mathbf{x} + h\mathbf{e}_j, t) + S(\mathbf{x} - h\mathbf{e}_j, t) \right] + O\left(\tau^2\right). \qquad \text{(A.3)}$$

Expanding $S(\mathbf{x}, t)$ about $\mathbf{x}$ yields:

$$S\big(\mathbf{x} \pm h\mathbf{e}_j, t\big) = S(\mathbf{x}, t) \pm hS_{x_j}(\mathbf{x}, t) + \frac{h^2}{2}\frac{\partial^2}{\partial x_j^2}S(\mathbf{x}, t) + O\Big(h^3\Big), \tag{A.4}$$

so

$$S\big(\mathbf{x} + h\mathbf{e}_j, t\big) + S\big(\mathbf{x} - h\mathbf{e}_j, t\big) = 2S(\mathbf{x}, t) + h^2\frac{\partial^2}{\partial x_j^2}S(\mathbf{x}, t) + O\Big(h^3\Big), \tag{A.5}$$

and (A.3) can be written as:

$$S(\mathbf{x}, t) + \tau\frac{\partial}{\partial t}S(\mathbf{x}, t) = S(\mathbf{x}, t) + \frac{h^2}{2n}\sum_{j=1}^{n}\left[\frac{\partial^2}{\partial x_j^2}S(\mathbf{x}, t)\right] + O\Big(\tau^2\Big) + O\Big(h^3\Big). \tag{A.6}$$

Rearranging terms and dividing both sides of (A.6) by $\tau$ yields:

$$\frac{\partial}{\partial t}S(\mathbf{x}, t) - \frac{1}{2n}\frac{h^2}{\tau}\sum_{j=1}^{n}\left[\frac{\partial^2}{\partial x_j^2}S(\mathbf{x}, t)\right] = O(\tau) + O\left(\frac{h^3}{\tau}\right). \tag{A.7}$$

Taking the limit of both sides of (A.7) as $h$ and $\tau$ approach zero while $\frac{h^2}{\tau}$ is fixed at 1 yields:

$$\frac{\partial}{\partial t}S(\mathbf{x}, t) - \frac{1}{2n}\Delta S(\mathbf{x}, t) = 0, \tag{A.8}$$

where $\Delta$ is the spatial Laplacian. (A.8) now applies for all $\mathbf{x} \in \Omega$ and $t \geq 0$. Note that $T_B = 0$ on the boundary, so $S(\mathbf{x}, t) = 0$ for $\mathbf{x} \in \partial\Omega$. Furthermore, $S(\mathbf{x}, 0) = 1$ for any point on the interior, and hence, $S(\mathbf{x}, t)$ satisfies (III.2).

### A.1.2 Hitting Time Moments

This appendix establishes the moments of the hitting time inside a shape.

Recall (A.8):

$$\begin{aligned}\frac{\partial}{\partial t}S(\mathbf{x}, t) - \frac{1}{2n}\Delta S(\mathbf{x}, t) = 0, \quad \forall \mathbf{x} \in \Omega, \quad t \geq 0,\\ S(\mathbf{x}, t) = 0, \quad \forall \mathbf{x} \in \partial\Omega, \quad t \geq 0,\\ S(\mathbf{x}, 0) = 1, \quad \forall \mathbf{x} \in \Omega.\end{aligned} \tag{A.9}$$

Multiplying both sides by $kt^{k-1}$ yields:

$$kt^{k-1}\frac{\partial}{\partial t}S(\mathbf{x}, t) - \frac{1}{2n}kt^{k-1}\Delta S(\mathbf{x}, t) = 0. \tag{A.10}$$

We integrate (A.10) with respect to $t$ as follows:

$$\int_0^\infty kt^{k-1}\frac{\partial}{\partial t}S(\mathbf{x},t)dt - \int_0^\infty \frac{1}{2n}kt^{k-1}\Delta S(\mathbf{x},t)dt = 0. \tag{A.11}$$

Constants can be brought outside the integral, as can the spatial Laplacian operator:

$$k\int_0^\infty t^{k-1}\frac{\partial}{\partial t}S(\mathbf{x},t)dt - \frac{1}{2n}k\Delta\int_0^\infty t^{k-1}S(\mathbf{x},t)dt = 0. \tag{A.12}$$

Recall from (III.5):

$$U_k(\mathbf{x}) = k\int_0^\infty t^{k-1}S(\mathbf{x},t)\,dt. \tag{A.13}$$

Substituting this into the second term of (A.12) yields:

$$k\int_0^\infty t^{k-1}\frac{\partial}{\partial t}S(\mathbf{x},t)dt - \frac{1}{2n}\Delta U_k(\mathbf{x}) = 0. \tag{A.14}$$

The first term of (A.14) can be integrated by parts as follows:

$$\begin{aligned}
k\int_0^\infty t^{k-1}\frac{\partial}{\partial t}S(\mathbf{x},t)dt &= kt^{k-1}S(\mathbf{x},t)\Big|_0^\infty - k(k-1)\int_0^\infty t^{k-2}S(\mathbf{x},t)\,dt \\
&= k\lim_{t\to\infty} t^{k-1}S(\mathbf{x},t) - 0 - k(k-1)\int_0^\infty t^{k-2}S(\mathbf{x},t)\,dt \\
&= 0 - 0 - k(k-1)\int_0^\infty t^{k-2}S(\mathbf{x},t)\,dt \\
&= -k(k-1)\int_0^\infty t^{k-2}S(\mathbf{x},t)\,dt.
\end{aligned} \tag{A.15}$$

Note that the limit above $\lim_{t\to\infty} t^{k-1}S(\mathbf{x},t)$ is in an indeterminate form $(0\cdot\infty)$. This can be rewritten as $\lim_{t\to\infty}\frac{t^{k-1}}{\frac{1}{S(\mathbf{x},t)}}$, and by L'Hospital's Rule, after differentiating $k-1$ times, the limit is zero.

We can substitute (A.13) with $k$ replaced by $k-1$ into (A.15):

$$k\int_0^\infty t^{k-1}\frac{\partial}{\partial t}S(\mathbf{x},t)dt = -kU_{k-1}(\mathbf{x}),$$

and the integral becomes

$$\begin{aligned}
-\frac{1}{2n}\Delta U_k(\mathbf{x}) &= kU_{k-1}(\mathbf{x}), \quad \forall\mathbf{x}\in\Omega, \\
U_0(\mathbf{x}) &= 1, \quad \forall\mathbf{x}\in\Omega, \\
U_k(\mathbf{x}) &= 0, \quad \forall\mathbf{x}\in\partial\Omega,
\end{aligned} \tag{A.16}$$

for k= 1,2,....

Note that when $k=0$ , the zeroth moment of $U_0(\mathbf{x})=1$, as $E[T_B^0]=1$.

## A.2 Brownian Motion Augmented with Natural Lifetime

### A.2.1 Survival Function Boundary Value Problem

**Lemma 1.** *The survival function of the minimum of the hitting time and natural lifetime is equivalent to:*

$$S_\beta(\mathbf{x},t) = e^{-\frac{t}{\beta}} S(\mathbf{x},t). \tag{A.17}$$

*Proof.* The survival function of the minimum of the hitting time and natural lifetime $T_L$ is:

$$S_\beta(\mathbf{x},t) = P(T>t|X(0)=\mathbf{x}), \tag{A.18}$$

as defined in (IV.1). We define the density function of $T_L$ as:

$$\begin{aligned} f_{T_L}(s) &= \frac{d}{ds} P(T_L < s) && \text{(A.19)}\\ &= \frac{d}{ds}\left[1 - e^{-s/\beta}\right] && \text{(A.20)}\\ &= \frac{1}{\beta} e^{-s/\beta}, && \text{(A.21)} \end{aligned}$$

and the conditional density function of $T_L$ given $X(0)$ as:

$$f_{T_L|X(0)}(s) = \frac{d}{ds} P(T_L < s|X(0)=\mathbf{x}). \tag{A.22}$$

Conditioning on $T_L$ allows us to write (A.18) as:

$$S_\beta(\mathbf{x},t) = \int_0^\infty P(\min(T_L,T_B)>t|X(0)=\mathbf{x}, T_L=s) f_{T_L|X(0)}(s)\, ds. \tag{A.23}$$

Recall that the natural lifetime of the particle and its initial position, $T_L$ and $X(0)$ respectively, are independent. Also, the hitting time of the particle and the natural lifetime of the particle, $T_B$ and $T_L$, are independent of one another. So, (A.23) becomes:

$$S_\beta(\mathbf{x},t) = \int_0^\infty P(\min(s,T_B) > t|X(0)=\mathbf{x}) f_{T_L}(s)\, ds. \tag{A.24}$$

From (A.21), we have that $f_{T_L}(s) = \frac{1}{\beta} e^{-s/\beta}$, so (A.24) becomes:

$$S_\beta(\mathbf{x},t) = \frac{1}{\beta}\int_0^\infty P(\min(s,T_B) > t|X(0)=\mathbf{x}) e^{-s/\beta} ds. \tag{A.25}$$

Splitting the integral at $s = t$ gives:

$$\begin{aligned} S_\beta(\mathbf{x},t) = &\frac{1}{\beta}\int_0^t P(\min(s,T_B) > t|X(0)=\mathbf{x}) e^{-s/\beta} ds \\ &+ \frac{1}{\beta}\int_t^\infty P(\min(s,T_B) > t|X(0)=\mathbf{x}) e^{-s/\beta} ds. \end{aligned} \tag{A.26}$$

Notice that for $s \in [0,t]$, $P\left(\min\left(s,T_B\right) > t | X(0) = \mathbf{x}\right) = 0$, so (A.26) simplifies to:

$$S_\beta(\mathbf{x},t) = \int_t^\infty P\left(\min\left(s,T_B\right) > t | X(0) = \mathbf{x}\right) e^{-s/\beta} ds. \tag{A.27}$$

In the interval $s = [t,\infty]$ we have:

$$P\left(\min\left(s,T_B\right) > t | X(0) = \mathbf{x}\right) = P\left(T_B > t | X(0) = \mathbf{x}\right). \tag{A.28}$$

and so:

$$S_\beta(\mathbf{x},t) = \int_t^\infty P\left(T_B > t | X(0) = \mathbf{x}\right) e^{-s/\beta} ds.$$

$P\left(T_B > t | X(0) = \mathbf{x}\right)$ is independent of $s$ and can be moved outside the integral. Hence:

$$S_\beta(\mathbf{x},t) = P\left(T_B > t | X(0) = \mathbf{x}\right) \int_t^\infty e^{-s/\beta} ds. \tag{A.29}$$

Substituting (III.1) into (A.29) gives:

$$S_\beta(\mathbf{x},t) = S\left(\mathbf{x},t\right) \int_t^\infty e^{-s/\beta} ds. \tag{A.30}$$

We then evaluate the integral in (A.30) to obtain:

$$S_\beta(\mathbf{x},t) = e^{-t/\beta} S\left(\mathbf{x},t\right). \quad \square \tag{A.31}$$

Recall (III.2):

$$\begin{aligned} \mathcal{L}[S(\mathbf{x},t)] &= 0, \quad \forall \mathbf{x} \in \Omega, \quad t \geq 0, \\ S(\mathbf{x},t) &= 0, \quad \forall \mathbf{x} \in \partial\Omega, \quad t \geq 0, \\ S(\mathbf{x},0) &= 1, \quad \forall \mathbf{x} \in \Omega. \end{aligned}$$

This boundary value problem was established in Appendix A.1.1 for the survival function of the hitting time $T_L$ given that a particle undergoes Brownian motion beginning at point $\mathbf{x} \subset \Omega$ .

Now, we will define a similar boundary value problem for the case where the random walk is started at a point outside of the shape . First, note that:

$$\mathcal{L}\left[S_\beta(\mathbf{x},t)\right] = \frac{\partial}{\partial t} S_\beta(\mathbf{x},t) - \frac{1}{2n} \Delta S_\beta(\mathbf{x},t). \tag{A.32}$$

Substituting (A.31) into (A.32) yields the following:

$$\mathcal{L}\left[S_\beta(\mathbf{x},t)\right] = \frac{\partial}{\partial t} e^{-t/\beta} S\left(\mathbf{x},t\right) - \frac{1}{2n} \Delta e^{-t/\beta} S\left(\mathbf{x},t\right). \tag{A.33}$$

Differentiating the first term on the right hand side of (A.33) and exploiting the linearity of the spatial Laplacian gives:

$$\mathcal{L}\left[S_\beta(\mathbf{x},t)\right] = e^{-t/\beta}\frac{\partial}{\partial t}S\left(\mathbf{x},t\right) - \frac{1}{\beta}e^{-t/\beta}S\left(\mathbf{x},t\right) - \frac{1}{2n}\Delta e^{-t/\beta}S\left(\mathbf{x},t\right), \tag{A.34}$$

$$= e^{-t/\beta}\left[\frac{\partial}{\partial t}S\left(\mathbf{x},t\right) - \frac{1}{\beta}S\left(\mathbf{x},t\right) - \frac{1}{2n}\Delta S\left(\mathbf{x},t\right)\right]. \tag{A.35}$$

Recall (III.2), which states:

$$\frac{\partial}{\partial t}S(\mathbf{x},t) - \frac{1}{2n}\Delta S(\mathbf{x},t) = 0, \quad \forall \mathbf{x} \in \Omega, \quad t \geq 0.$$

Substituting for $S_\beta(\mathbf{x},t)$ into (A.35) gives:

$$\mathcal{L}\left\{S_\beta(\mathbf{x},t)\right\} = e^{-t/\beta}\left[-\frac{1}{\beta}S\left(\mathbf{x},t\right)\right].$$

This can be rewritten as a homogeneous partial differential equation:

$$\mathcal{L}\left\{S_\beta(\mathbf{x},t)\right\} + \frac{1}{\beta}e^{-t/\beta}S\left(\mathbf{x},t\right) = 0, \tag{A.36}$$

which, in light of (A.31), can be rewritten as:

$$\mathcal{L}\left\{S_\beta(\mathbf{x},t)\right\} + \frac{1}{\beta}S_\beta\left(\mathbf{x},t\right) = 0. \tag{A.37}$$

Recall from (III.2) the boundary condition $S\left(\mathbf{x},t\right) = 0$ and initial condition $S(\mathbf{x},0) = 1$. It is also true that $S_\beta\left(\mathbf{x},t\right) = 0$ when the initial position is on the boundary of the shape. In addition we have the initial condition $S_\beta(\mathbf{x},0) = 1$. Therefore, inside the shape, we have the following initial boundary value problem:

$$\begin{aligned}
\mathcal{L}\left\{S_\beta(\mathbf{x},t)\right\} + \frac{1}{\beta}S_\beta\left(\mathbf{x},t\right) = 0, \quad \forall \mathbf{x} \in \bar{\Omega}, \quad t \geq 0, \\
S_\beta(\mathbf{x},t) = 0, \quad \forall \mathbf{x} \in \partial\Omega, \quad t \geq 0, \\
S_\beta(\mathbf{x},0) = 1, \quad \forall \mathbf{x} \in \bar{\Omega}.
\end{aligned} \tag{A.38}$$

To define the initial boundary value problem outside the shape, we must add another boundary condition. For points sufficiently far from the shape boundary, the survival function $S_\beta(\mathbf{x},t)$ is equal to the survival function of the natural lifetime, $T_L$. That is,

$$\begin{aligned}
\lim_{\|\mathbf{x}\|\to\infty} S_\beta(\mathbf{x},t) &= P\left(T_L > t | X\left(0\right) = \mathbf{x}\right), \\
&= \int_t^\infty f_{T_L}\left(s\right) ds.
\end{aligned} \tag{A.39}$$

Since $T_L$ has an exponential distribution with expected value $\beta$, we can write (A.39) as:

$$\lim_{\|\mathbf{x}\|\to\infty} S_\beta(\mathbf{x},t) = e^{-t/\beta}. \tag{A.40}$$

Therefore, outside the shape we have the following initial boundary value problem:

$$\begin{aligned}
\mathcal{L}\{S_\beta(\mathbf{x},t)\} + \frac{1}{\beta}S_\beta(\mathbf{x},t) &= 0, \qquad \forall \mathbf{x}\in\mathbb{R}^n\backslash\bar{\Omega}, \quad t\geq 0,\\
S_\beta(\mathbf{x},t) &= 0, \qquad \forall \mathbf{x}\in\partial\Omega, \quad t\geq 0,\\
S_\beta(\mathbf{x},0) &= 1, \qquad \mathbf{x}\in\mathbb{R}^n\backslash\bar{\Omega},\\
\lim_{\|\mathbf{x}\|\to\infty} S_\beta(\mathbf{x},t) &= e^{-t/\beta}, \quad \forall \mathbf{x}\in\mathbb{R}^n\backslash\bar{\Omega}, \quad t\geq 0.
\end{aligned} \tag{A.41}$$

Hence, $S_\beta(\mathbf{x},t)$ is defined over all $\mathbb{R}^n$ by (A.38) and (A.41).

### A.2.2 Moments of the Survival Function

In this section the $k$th moments of $T$ are established. Moments of $S_\beta(\mathbf{x},t)$ are denoted by $U_{k,\beta}(\mathbf{x})$, and the $k^{th}$ moment can be computed from the survival function by:

$$U_{k,\beta}(\mathbf{x}) = k\int_0^\infty t^{k-1}S_\beta(\mathbf{x},t)\ dt, \tag{A.42}$$

for $k = 1, 2, \ldots$. Multiplying each side of (IV.2) by $kt^{k-1}$ and integrating yields:

$$k\int_0^\infty t^{k-1}\frac{\partial}{\partial t}S_\beta(\mathbf{x},t)\,dt - k\int_0^\infty t^{k-1}\frac{1}{2n}\Delta S_\beta(\mathbf{x},t)\,dt + \frac{k}{\beta}\int_0^\infty t^{k-1}S_\beta(\mathbf{x},t)\,dt = 0. \tag{A.43}$$

When $k = 1$, the first term in (A.43) simplifies to $-1$. For $k > 1$ the first term in (A.43) can be integrated by parts, as follows:

$$k\int_0^\infty t^{k-1}\frac{\partial}{\partial t}S_\beta(\mathbf{x},t)\,dt = k\left(t^{k-1}S_\beta(\mathbf{x},t)\right)\Big|_0^\infty - k(k-1)\int_0^\infty t^{k-2}S_\beta(\mathbf{x},t)\,dt, \tag{A.44}$$

$$= k\left(\lim_{t\to\infty} t^{k-1}S_\beta(\mathbf{x},t) - 0\right) - kU_{k-1,\beta}(\mathbf{x}). \tag{A.45}$$

Using (A.42),

$$\lim_{t\to\infty} t^{k-1}S_\beta(\mathbf{x},t) = 0,$$

and therefore,

$$k\int_0^\infty t^{k-1}\frac{\partial}{\partial t}S_\beta(\mathbf{x},t)\,dt = -kU_{k-1,\beta}(\mathbf{x}). \tag{A.46}$$

To integrate the second term in (A.43), we exercise the linearity property of the Laplacian to write:

$$k\int_0^\infty t^{k-1}\frac{1}{2n}\Delta S_\beta(\mathbf{x},t)\,dt = \frac{k}{2n}\Delta\int_0^\infty t^{k-1}S_\beta(\mathbf{x},t)\,dt, \tag{A.47}$$

$$= \frac{1}{2n}\Delta U_{k,\beta}(\mathbf{x})\,dt. \tag{A.48}$$

Finally, the third term in (A.43) can be simplified by applying (A.42) , i.e.,

$$\frac{k}{\beta}\int_0^\infty t^{k-1}S_\beta\left(\mathbf{x},t\right)dt = \frac{1}{\beta}U_{k,\beta}(\mathbf{x})\,. \tag{A.49}$$

Combining the three terms from (A.43) yields the following boundary value problem:

$$\begin{aligned} -kU_{k-1,\beta}(\mathbf{x}) - \frac{1}{2n}\Delta U_{k,\beta}(\mathbf{x}) + \frac{1}{\beta}U_{k,\beta}(\mathbf{x}) = 0, \quad \forall\mathbf{x}\in\mathbb{R}^n\backslash\partial\Omega,\\ U_{k,\beta}(\mathbf{x}) = 0, \quad \forall\mathbf{x}\in\partial\Omega,\\ U_{0,\beta}(\mathbf{x}) = 1, \quad \forall\mathbf{x}\in\mathbb{R}^n. \end{aligned} \tag{A.50}$$

Introducing the natural lifetime of the random walk allows for the mean dying time to be computed for Brownian motion beginning at a point outside the shape boundary. Without the addition of the natural lifetime, the Brownian motion had the potential to continue infinitely if it began outside the shape boundary. In order to solve (IV.26) we must specify boundary conditions for points on the image boundary. Denote the image interior $I$ and the image boundary $\partial I$.

We impose Dirichlet boundary conditions such that the expected value of the lifetime of the random walks beginning on the boundary of the shape is equal to the natural lifetime of the random walk.

Similar to (A.41) we have:

$$\lim_{\|\mathbf{x}\|\to\infty} U_{1,\beta}(\mathbf{x},t) = \beta, \tag{A.51}$$

where $\beta = \frac{1}{\lambda}$, the expected value of $T_L$. To define the region outside the shape, assume that the shape, $\bar{\Omega}$, is contained in an image $I$. In addition, assume that $I$ is sufficiently large such that the value $\beta$ is reached on $\partial I$. With the addition of the boundary conditions, (A.50) becomes:

$$-kU_{k-1,\beta}(\mathbf{x}) - \frac{1}{2n}\Delta U_{k,\beta}(\mathbf{x}) + \frac{1}{\beta}U_{k,\beta}(\mathbf{x}) = 0 \qquad \forall \mathbf{x} \in I,$$
$$U_{1,\beta}(\mathbf{x}) = \beta \qquad \forall \mathbf{x} \in \partial I, \tag{A.52}$$

where $\beta$ is the expected value of exponentially distributed random variable $T_L$ the natural lifetime of the particle.

Setting $k = 1$ gives an equation for the first moment, or the expected value, of T given $X(0) = x$:

$$-U_{0,\beta}(\mathbf{x}) - \frac{1}{2n}\Delta U_{1,\beta}(\mathbf{x}) + \frac{1}{\beta}U_{1,\beta}(\mathbf{x}) = 0. \tag{A.53}$$

$U_{0,\beta}(x)$ is the zeroth moment of $S_\beta(\mathbf{x}, t)$, which is equal to 1. Substituting and rearranging gives:

$$\frac{1}{\beta}U_{1,\beta}(\mathbf{x}) - \frac{1}{2n}\Delta U_{1,\beta}(\mathbf{x}) = 1. \tag{A.54}$$

### A.2.3 Mean Dying Time on a Circle

In this section we will establish $U_{k,\beta}(x)$, the $k^{th}$ moment of the survival function with parameter $\beta$ on a circle with radius $R$.

Recall (IV.5):

$$-kU_{k-1,\beta}(\mathbf{x}) - \frac{1}{2n}\Delta U_{k,\beta}(\mathbf{x}) + \frac{1}{\beta}U_{k,\beta}(\mathbf{x}) = 0, \quad \forall \mathbf{x} \in \mathbb{R}^n \backslash \partial\Omega,$$
$$U_{k,\beta}(\mathbf{x}) = 0, \quad \forall \mathbf{x} \in \partial\Omega,$$
$$U_{0,\beta}(\mathbf{x}) = 1, \quad \forall \mathbf{x} \in \mathbb{R}^n.$$

If $\Omega$ is a sphere of radius R, then define:

$$Y_{k,\beta}(r) = Y_{k,\beta}(\|\mathbf{x}\|) = U_{k,\beta}(\mathbf{x}). \tag{A.55}$$

Then, we have:

$$-kY_{k-1,\beta}(r) - \frac{1}{2n}\left[Y''_{k,\beta}(r) + \frac{(n-1)}{r}Y'_{k,\beta}(r)\right] + \frac{1}{\beta}Y_{k,\beta}(r) = 0. \tag{A.56}$$

The first moment in two dimensions is found as follows:

$$-Y_{0,\beta}(r) - \frac{1}{4}\left[Y''_{1,\beta}(r) + \frac{1}{r}Y'_{1,\beta}(r)\right] + \frac{1}{\beta}Y_{1,\beta}(r) = 0. \tag{A.57}$$

Noting $Y_{0,\beta}(r) = 1$, this simplifies to:

$$-\frac{1}{4}\left[Y''_{1,\beta}(r) + \frac{1}{r}Y'_{1,\beta}(r)\right] + \frac{1}{\beta}Y_{1,\beta}(r) = 1. \tag{A.58}$$

The solution to this differential equation is:

$$Y_{1,\beta}(r) = c_1 J_0\left(\frac{2ir}{\sqrt{\beta}}\right) + c_2 Y_0\left(\frac{-2ir}{\sqrt{\beta}}\right) + \beta, \tag{A.59}$$

where $J_1$ is a Bessel function of the first kind and $Y_1$ is a Bessel function of the second kind.

It follows that:

$$Y'_{1,\beta}(r) = \frac{2i}{\sqrt{\beta}}\left[c_2 Y_1\left(\frac{-2ir}{\sqrt{\beta}}\right) - c_1 J_1\left(\frac{2ir}{\sqrt{\beta}}\right)\right].$$

Applying the initial condition $Y'_{1,\beta}(0) = 0$ gives:

$$\begin{aligned} Y'_{1,\beta}(0) &= c_1 J_1(0) + c_2 Y_1(0), \\ &= c_2 Y_1(0), \end{aligned}$$

and therefore it is true that $c_2 = 0$. (A.59) then becomes:

$$Y_{1,\beta}(r) = c_1 J_0\left(\frac{2ir}{\sqrt{\beta}}\right) + \beta. \tag{A.60}$$

Applying the second boundary condition $U_{1,\beta}(R) = 0$ gives:

$$0 = c_1 J_0\left(\frac{2iR}{\sqrt{\beta}}\right) + \beta, \tag{A.61}$$

$$c_1 = \frac{-\beta}{J_0\left(\frac{2iR}{\sqrt{\beta}}\right)}. \tag{A.62}$$

(A.63) becomes:

$$Y_{1,\beta}(r) = \beta - \frac{\beta}{J_0\left(\frac{2iR}{\sqrt{\beta}}\right)} J_0\left(\frac{2ir}{\sqrt{\beta}}\right), \tag{A.63}$$

where $J_0$ is a Bessel function of the first kind and can alternately be expressed as:

$$Y_{1,\beta}(r) = \beta - \frac{\beta}{I_0\left(\frac{2R}{\sqrt{\beta}}\right)} I_0\left(\frac{2r}{\sqrt{\beta}}\right), \tag{A.64}$$

where $I_0$ is a modified Bessel function of the first kind.

Now, we show that (IV.31) is a solution to equation (IV.5) outside a circle of radius R.

Recall (A.58):

$$-\frac{1}{4}\left[Y''_{1,\beta}(r) + \frac{1}{r}Y'_{1,\beta}(r)\right] + \frac{1}{\beta}Y_{1,\beta}(r) = 1 \tag{A.65}$$

and (IV.31):

$$Y_{1,\beta}(r) = \beta - \frac{\beta}{K_0\left(\frac{2R}{\sqrt{\beta}}\right)} K_0\left(\frac{2r}{\sqrt{\beta}}\right), \tag{A.66}$$

The first and second derivatives of (IV.31) are:

$$Y'_{1,\beta}(r) = \frac{2\sqrt{\beta}}{K_0\left(\frac{2R}{\sqrt{\beta}}\right)} K_1\left(\frac{2r}{\sqrt{\beta}}\right), \tag{A.67}$$

and

$$Y''_{1,\beta}(r) = \frac{-2}{K_0\left(\frac{2R}{\sqrt{\beta}}\right)}\left[K_0\left(\frac{2r}{\sqrt{\beta}}\right) + K_2\left(\frac{2r}{\sqrt{\beta}}\right)\right], \tag{A.68}$$

respectively.

Substituting into equation (A.58) yields:

$$-\frac{1}{4}\left[\frac{-2\left[K_0\left(\frac{2r}{\sqrt{\beta}}\right) + K_2\left(\frac{2r}{\sqrt{\beta}}\right)\right]}{K_0\left(\frac{2R}{\sqrt{\beta}}\right)} + \frac{2\sqrt{\beta}}{r}\frac{K_1\left(\frac{2r}{\sqrt{\beta}}\right)}{K_0\left(\frac{2R}{\sqrt{\beta}}\right)}\right] - \frac{K_0\left(\frac{2r}{\sqrt{\beta}}\right)}{K_0(\frac{2R}{\sqrt{\beta}})} = 0, \tag{A.69}$$

$$\frac{K_0\left(\frac{2r}{\sqrt{\beta}}\right) + K_2\left(\frac{2r}{\sqrt{\beta}}\right)}{2K_0\left(\frac{2R}{\sqrt{\beta}}\right)} - \frac{\sqrt{\beta}}{2r}\frac{K_1\left(\frac{2r}{\sqrt{\beta}}\right)}{K_0\left(\frac{2R}{\sqrt{\beta}}\right)} - \frac{K_0\left(\frac{2r}{\sqrt{\beta}}\right)}{K_0(\frac{2R}{\sqrt{\beta}})} = 0. \tag{A.70}$$

Multiplying by $2K_0\left(\frac{2R}{\sqrt{\beta}}\right)$ gives:

$$K_0\left(\frac{2r}{\sqrt{\beta}}\right) + K_2\left(\frac{2r}{\sqrt{\beta}}\right) - \frac{\sqrt{\beta}}{r}K_1\left(\frac{2r}{\sqrt{\beta}}\right) - 2K_0\left(\frac{2r}{\sqrt{\beta}}\right) = 0.$$

Combining like terms gives:

$$K_2\left(\frac{2r}{\sqrt{\beta}}\right) - K_0\left(\frac{2r}{\sqrt{\beta}}\right) - \frac{\sqrt{\beta}}{r}K_1\left(\frac{2r}{\sqrt{\beta}}\right) = 0.$$

Since

$$K_2\left(\frac{2r}{\sqrt{\beta}}\right) - K_0\left(\frac{2r}{\sqrt{\beta}}\right) = \frac{\sqrt{\beta}}{r}K_1\left(\frac{2r}{\sqrt{\beta}}\right),$$

the equation holds. (IV.31) also satisfies the boundary conditions $\lim_{r\to\infty} Y_{1,\beta}(r) = \beta$ and $Y_{1,\beta}(R) = 0$.

---

# References


[1] D. Baja, G. Sanniti, and E. Thiel (1996). Skeletonization algorithm running on path-based distance maps. *Image and vision Computing*, 14.1: 47-57.

[2] M. Bhardwaj, H. Tulsani, S. Rajput (2014). Features Extraction by using Poisson Equation. *International Journal of Research in Advent Technology*, Vol.2, No.5.

[3] I. Biederman (1987). Recognition-by-components: a theory of human image understanding. *Psychological review*, 94.2: 115.

[4] M. Blank, L. Gorelick, E. Shechtman, M. Irani, R. Basri (2005). Actions as Space-Time Shapes. *Proceedings of the Tenth IEEE International Conference on Computer Vision*, Identification.

[5] H. Blum (1967). A transformation for extracting new descriptors of shape. *Models for the perception of speech and visual form*, 19.5: 362-380.

[6] H. Blum and H.-H. Nagel. (1978). Shape description using weighted symmetry axis features. *Pattern Recognition*, 10:167-180.

[7] A.M. Bronstein, M. M. Bronstein, and R. Kimmel (2007). Expression-invariant representations of faces. *Image Processing, IEEE Transactions on*, 16.1: 188-197.

[8] Y. Chahir, Y. Zinbi, M. Ghoniem, A. Elmoataz (2009). A random walk through human behavior. *Proceedings of IS&T/SPIE International Conference on Multimedia Content Access: Algorithms and Systems III*, Vol. 7255. 2009.

[9] A. Elad and R. Kimmel (2003). On bending invariant signatures for surfaces. *Pattern Analysis and Machine Intelligence, IEEE Transactions on*, 25.10 (2003): 1285-1295.

[10] R. Fabbri, L. D. F. Costa, J. C. Torelli, O. M. Bruno (2008). 2D Euclidean distance transform algorithms: A comparative survey. *ACM Computing Surveys (CSUR)*, 40(1), 2.

[11] R. Fabbri, L. F. Estrozi and L. Da F. Costa. (2002). On Voronoi diagrams and medial axes. *Journal of Mathematical Imaging and Vision*, 17.1: 27-40.

[12] P.T. Fletcher (2004). Principal geodesic analysis for the study of nonlinear statistics of shape. *Medical Imaging, IEEE Transactions on*, 23.8: 995-1005.

[13] L. Gorelick and R. Basri (2009). Shape based detection and top-down delineation using image segments. *International journal of computer vision*, 83.3: 211-232.

[14] L. Gorelick, M. Galun, E. Sharon, R. Basri, and A. Brandt (2006). Shape Representation and Classification Using the Poisson Equation. *IEEE Transactions on Pattern Analysis and Machine Intelligence*, 28.12 (2006): 1991-2005.

[15] L. Grady (2006). Random Walks for Image Segmentation. *IEEE Transactions on Pattern Analysis and Machine Intelligence*, Vol. 28, No. 11, Nov. 2006.

[16] Y. LeCun (1998). The MNIST Database of Handwritten Digits. *http://yann.lecun.com/exdb/mnist/*.

[17] W. Ma, F. Wu and M. Ouhyoung (2003). Skeleton extraction of 3D objects with radial basis functions. *IEEE Shape Modeling International 2003*.

[18] C. Maes, T. Fabry, J. Keustermans, D. Smeets, P. Suetens and D. Vandermeulen (2010). Feature detection on 3D face surfaces for pose normalisation and recognition. *IEEE*, Biometrics: Theory Applications and Systems (BTAS), 2010 Fourth IEEE International Conference on.

[19] D. Marr, H. K. Nishihara (1978). Representation and Recognition of the Spatial Organization of Three-Dimensional Shapes. *Proceedings of the Royal Society of London. Series B, Biological Sciences*, Vol. 200, No. 1140 pp. 269-294.

[20] N. Mayya and V. T. Rajan (1996). Voronoi diagrams of polygons: A framework for shape representation. *Journal of Mathematical Imaging and Vision*, 6.4: 355-378.

[21] R. Ogniewicz and M. Ilg.(1992). Voronoi skeletons: Theory and applications. *IEEE*, Proceedings CVPR'92., 1992 IEEE Computer Society Conference on.

[22] K. Palagyi and A. Kuba (1998). A 3D 6-subiteration thinning algorithm for extracting medial lines. *Pattern Recognition Letters*, 19.7: 613-627.

[23] A. P. Pentland (1987). Recognition by parts. *SRI International Menlo Park CA Computer and Information Sciences Div.*, No. SRI-TR-406.

[24] S. M. Pizer, et al. (2003). Deformable m-reps for 3D medical image segmentation. *International Journal of Computer Vision*, 55.2-3: 85-106.

[25] S. M. Pizer, D. S. Fritsch, P. A. Yushkevich, V. E. Johnson, E. L. Chaney. (1999). Segmentation, registration, and measurement of shape variation via image object shape. *Medical Imaging, IEEE Transactions on*, 18.10 (1999): 851-865.

[26] M. Rao, et al. (2005). Comparison of human and automatic segmentations of kidneys from CT images. *International Journal of Radiation Oncology* Biology* Physics*, 61.3: 954-960.

[27] D. Shaked and A. M. Bruckstein (1998). Pruning medial axes. *Computer vision and image understanding*, 69.2: 156-169.

[28] K. Siddiqi and B. B. Kimia. (1995). Parts of visual form: Computational aspects. *Pattern Analysis and Machine Intelligence, IEEE Transactions on*, 17.3: 239-251.

[29] M. Styner and G. Gerig (2000). Hybrid boundary-medial shape description for biologically variable shapes. *IEEE*, Mathematical Methods in Biomedical Image Analysis, 2000. Proceedings. IEEE Workshop on.

[30] L.R. Williams and D. W. Jacobs (1997). Stochastic completion fields: A neural model of illusory contour shape and salience. *Neural Computation* , 9.4: 837-858.

[31] L. Yen, D. Vanvyve, F. Wouters, F. Fouss, M. Verleysen and M. Saerens (2005). Clustering using a random walk based distance measure. *European Symposium on Artificial Neural Networks*, April 2005.

[32] P. Yogarajah, J.V. Condell, G. Prasad (2011). PRWGEI: Poisson random walk based gait recognition. *Image and Signal Processing and Analysis (ISPA), 7th International Symposium on*.

[33] Y. Zhou, A. Kaufman, and A. W. Toga (1998). Three-dimensional skeleton and centerline generation based on an approximate minimum distance field. *The Visual Computer*, 14.7: 303-314.